

M Keilhacker et al

High Fusion Performance from Deuterium-Tritium Plasmas in JET

"This document is intended for publication in the open literature. It is made available on the understanding that it may not be further circulated and extracts may not be published prior to publication of the original, without the consent of the Publications Officer, JET Joint Undertaking, Abingdon, Oxon, OX14 3EA, UK".

"Enquiries about Copyright and reproduction should be addressed to the Publications Officer, JET Joint Undertaking, Abingdon, Oxon, OX14 3EA".

High Fusion Performance from Deuterium-Tritium Plasmas in JET

M Keilhacker, A Gibson, C Gormezano, P Lomas, P R Thomas,
M L Watkins, P Andrew, B Balet, D Borba, C D Challis,
I Coffey, G A Cottrell, H P L De Esch, N Deliyannis, A Fasoli,
C W Gowers, H Y Guo, G T A Huysmans, T T C Jones,
W Kerner, R T W König, M J Loughlin, A Maas, F Marcus,
M F F Nave, F G Rimini, G Sadler, S Sharapov, G Sips,
P Smeulders, F Söldner, A Taroni, B J D Tubbing,
M G von Hellermann, D J Ward,
and the JET Team[§].

JET Joint Undertaking, Abingdon, Oxfordshire, OX14 3EA,

§ See Appendix I

Preprint of a Paper to be submitted for publication in Nuclear Fusion

October 1998

ABSTRACT

High fusion power experiments using D-T mixtures in ELM-free H-mode and optimised shear regimes in JET are reported. A fusion power of 16.1 MW has been produced in an ELM-free H-mode at 4.2 MA / 3.6 T. The transient value of the fusion amplification factor was 0.95 ± 0.17 , consistent with the high value of $n_{DT}(0) \tau_E^{dia} T_i(0) = 8.7 \times 10^{20} \text{ m}^{-3} \text{ s keV} \pm 20\%$, and maintained for about half an energy confinement time until excessive edge pressure gradients resulted in discharge termination by MHD instabilities. The ratio of D-D and D-T fusion powers (from separate but otherwise similar discharges) showed the expected factor of 210, validating D-D projections of D-T performance for similar pressure profiles and good plasma mixture control which was achieved by loading the vessel walls with the appropriate D-T mix. Magnetic fluctuation spectra showed no evidence of Alfvénic instabilities driven by alpha particles, in agreement with theoretical model calculations. Alpha particle heating has been unambiguously observed, its effect being separated successfully from possible isotope effects on energy confinement by varying the tritium concentration in otherwise similar discharges. The scan showed that there was no or at most a very weak isotope effect on the energy confinement time. The highest electron temperature was clearly correlated with the maximum alpha particle heating power and the optimum D-T mixture; the maximum increase was $1.3 \pm 0.23 \text{ keV}$ with 1.3 MW of alpha particle heating power, consistent with classical expectations for alpha particle confinement and heating. In the optimised shear regime, clear internal transport barriers were established for the first time in D-T, with a power similar to that required in D-D. The ion thermal conductivity in the plasma core approached neoclassical levels. Real time power control maintained the plasma core close to limits set by pressure gradient driven MHD instabilities, allowing 8.2 MW of D-T fusion power with $n_{DT}(0) \tau_E^{dia} T_i(0) \approx 10^{21} \text{ m}^{-3} \text{ s keV}$, even though full optimisation was not possible within the imposed neutron budget. In addition, quasi steady-state discharges with simultaneous internal and edge transport barriers have been produced with high confinement and a fusion power of up to 7 MW; these double barrier discharges show a great potential for steady-state operation.

1. INTRODUCTION

Significant controlled fusion power was first produced during the Preliminary Tritium Experiment (PTE) in the Joint European Torus (JET) in 1991 [1], when a hot ion H-mode plasma containing 11% tritium in deuterium produced 2 MJ of fusion energy with a peak fusion power $P_{DT} = 1.7 \text{ MW}$ and a fusion power gain $Q_{in} = P_{DT}/P_{in} = 0.12$, P_{in} being the total input power to the torus. Tritium usage and neutron production were deliberately kept low during the PTE in order to limit vessel activation so that a pumped divertor [2] could be installed three months later during a manned intervention. This was the first of a series of divertors installed in JET between 1991 and 1996 to test the effect of increasing geometric closure on divertor behaviour and plasma

performance with deuterium plasmas closest in scale and geometry to that foreseen for the International Thermonuclear Experiment Reactor (ITER) [3].

Meanwhile, the Tokamak Fusion Test Reactor (TFTR) in the USA operated in deuterium-tritium (D-T) mixtures and, using 50% of D and 50% of T, produced 10.7 MW of fusion power and a fusion gain $Q_{in}=0.27$ in the supershot regime [4]. This limiter tokamak also explored improved confinement in the enhanced reversed shear (ERS) regime, but the performance improvements achieved in deuterium [5] could not be translated into D-T [4, 6].

With the closure of TFTR in April 1997, JET is now the only fusion experiment able to operate with D-T fuel mixtures. Furthermore, and going beyond TFTR, JET has an effective divertor and can operate in a wider range of plasma regimes. In addition, JET has the first industrial scale plant for the closed cycle supply and processing of tritium (the Active Gas Handling System, AGHS [7]), together with a proven remote handling capability. These have allowed the JET programme for the period to the end of 1999 to include both a broad-based series of D-T experiments (DTE1) to address crucial issues of D-T physics and technology for ITER, and the development and exploration of divertor concepts for ITER.

During DTE1, the JET torus was pumped continuously through the AGHS and was supplied with D-T by the gas introduction and neutral beam (NB) systems. The tritium was stored in uranium beds and re-processed in the AGHS to a purity of 99.4% by gas chromatography. In contrast to the PTE, when the total amount of tritium available was 0.2 g, there was no equivalent restriction for DTE1. The site inventory of 20 g of tritium was re-processed eight times by the AGHS, making the equivalent of 99.3 g of tritium available for DTE1.

The fusion energy produced was 675 MJ, equivalent to the limit set at this stage in the JET programme on the total neutron production of less than 2.5×10^{20} neutrons (compared to the limit of about 1.5×10^{18} neutrons imposed for the PTE) so that the subsequent activation of the JET vessel would not prevent manned in-vessel intervention for more than a year after the end of DTE1. The JET programme continued after DTE1 with an ITER Urgent Physics Phase and the remote handling replacement of the relatively closed Mark IIAP divertor [8] used during DTE1 by an even more closed 'gas box' divertor (Mark IIGB).

The physics objectives of DTE1 can be divided into two areas. The first, discussed in a companion paper [9], was the characterisation of the baseline ITER mode of operation, the steady-state ELMy H-mode, in D-T. Of particular importance were assessments of the hydrogen isotope effects on the H-mode threshold power, the energy confinement and the edge operational space, of various heating schemes at the ion cyclotron resonance frequency (ICRF) in D-T plasmas, and of high fusion power and Q in steady-state.

The aims of the second area, which is the subject of this paper, were to produce maximum fusion power and Q, to observe alpha particle heating and to study the stability of Alfvén Eigenmodes. These aims are inter-related since high fusion power corresponds to high alpha particle pressure, thereby maximising the effect of the alpha particles for heating and destabilising of Alfvén Eigenmodes.

In D-D plasmas on JET, two modes of operation have consistently out-performed, at least transiently, the ELMy H-mode by a factor of about four in fusion performance. These are the hot ion ELM-free H-mode, which had already been tested in the PTE and was considered to be the established route to high performance, and the optimised shear mode, which had been developed during the year leading up to DTE1. Their translation from D-D to D-T is of great interest for understanding these regimes as well as producing high performance. There is also a long term interest in developing the latter regime towards steady state.

These high performance discharges predominantly use high energy NB injection to heat and fuel the plasmas. During DTE1, the JET NB system was operated with tritium in all eight beam sources of one of the two injectors. More than 10 MW of tritium NB power was delivered at voltages of ≈ 155 kV, for pulse durations ≤ 5 s. The other injector operated exclusively in deuterium at ≈ 78 kV. ICRF was used to supplement NB heating.

The experimental set-up, the heating systems and the D-T related diagnostics are discussed in more detail in the companion paper [9].

The paper is structured as follows. Section 2 considers the technical issues related to tritium plasma concentrations, tritium retention in the vessel wall and clean-up. The questions of fusion power performance (including the stability of Alfvén Eigenmodes) and the detection of alpha particle heating in the ELM-free H-mode are then addressed in Sections 3 and 4, respectively. Section 5 considers fusion power performance and physics in the optimised shear regime. The summary, conclusions and outlook follow in Section 6.

2. TRITIUM CONCENTRATIONS, VESSEL RETENTION AND CLEAN-UP

During DTE1 over 200 pulses had plasma tritium concentrations greater than 40%. Control of the isotopic mixture in the plasma was achieved by preceding the experiment with a few ohmic or ICRF heated pulses to changeover the isotopic composition of the walls. With 100% tritium fuelling, plasma tritium concentrations greater than 90% were readily obtained (Fig. 1a).

During the campaign, it was possible to achieve nearly complete tritium recovery ($>98\%$) from the NB injector which operated in tritium. However, about 30% of the tritium input to the torus was retained in the torus (Fig. 1b). After the tritium experiments were completed, the experimental campaign continued with about 2 months of operation in deuterium and hydrogen, after which the torus tritium inventory had fallen to 17% of the torus input (6 g). The plasma tritium concentrations had fallen to $\approx 0.1\%$ by this time, so it was clear that the tritium inventory in the torus was not contributing significantly to the isotopic mixture.

The torus tritium inventory at the end of DTE1 was over 3 times larger than had been expected from the tritium retention results of the PTE [10]. For the purposes of using the PTE results to extrapolate to DTE1, a simple analytical fit to the PTE data was used to represent the behaviour of retained tritium after each pulse. While this PTE-based prediction closely followed the tritium concentrations, the difference in actual and predicted tritium inventories grew over

the course of the campaign. This suggests that there was a sink for tritium during DTE1 which was not present at the time of the PTE.

The high level of tritium retention during DTE1 has been related to carbon films, saturated with deuterium and tritium and located in the divertor. While co-deposited films have always been present in the JET vessel, the films with the Mark IIA divertor were unprecedentedly thick and hydrogen rich. The films were found in cold regions of the divertor, shadowed from direct contact with the plasma. While the majority of the JET vessel was heated to 320°C, these cold regions are actively cooled to ≈50°C (they act as a heat shield to protect the in-vessel divertor coils), allowing the formation of stable films with more than 40% hydrogen concentrations in carbon [11]. In contrast, at the time of the PTE (i.e. before the installation of a divertor), the whole vessel interior was maintained at 300°C. The films which formed on water-cooled metal surfaces were found to flake off, probably on venting, leading to considerable debris in the bottom of the divertor. Even though the hardware is similar on the inner and outer legs of the divertor, the flakes were found only on the inner leg.

The processes leading to this asymmetry and the high level of carbon erosion needed to form the films are still under investigation. Analysis of tiles and flakes removed from the vessel after the experimental campaign is underway and expected to identify the exact location of the tritium inventory still inside the vessel. This analysis will also determine the physical and chemical characteristics of the films.

3. THE ELM-FREE H-MODE

The ELM-free H-mode has been developed in JET over a wide range of plasma currents (1.7-4.2 MA) and toroidal magnetic fields (1.7-3.8 T) with three different divertor configurations. It has been the established route to high fusion performance in deuterium and was successfully used for the PTE [1]. High values of the fusion triple product, $n_{DT}(0)\tau_E T_i(0)$, were

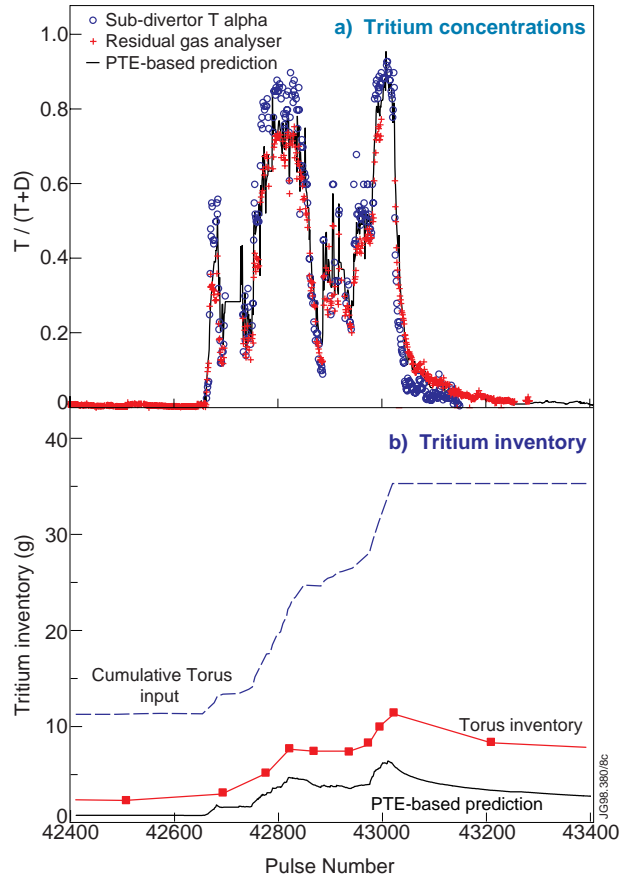


FIG. 1. (a) Tritium concentrations and (b) tritium inventory for the second period of DTE1 from September to November 1997 (Pulses No. 42661 to 43023). Note that there had already been a first period of D-T operation in May/June 1997. The tritium concentrations shown were measured by sampling neutrals in the sub-divertor volume during pulses, and sampling gas by residual gas analysis between pulses. The PTE-based prediction is based on exhaust measurements during the PTE.

observed and transient $Q_{DT} \approx 1$ (as defined in [1]) was suggested on the basis of TRANSP extrapolations from pure deuterium plasmas to 50:50 D-T mixtures [12]. In the PTE the regime was thought to be limited by the power handling of the divertor target tiles through the occurrence of a carbon impurity “bloom” [1]. Following the installation of the Mark I pumped divertor [2], which had sufficient power handling capability to avoid blooms, it was recognised that the performance limitations were of MHD origin [13] and that highly shaped plasmas, high plasma current and low recycling were necessary to maximise the ELM-free period [14]. However, outer modes [13], identified as external kinks associated with high edge bootstrap currents [15], could still degrade performance, but could be ameliorated by ramping down the plasma current.

3.1. The D-D Experience and Extrapolation to D-T

In order to permit a comparison between the fusion performance in D-D and D-T it is first necessary to discuss how deuterium discharges were expected to translate to D-T.

Despite the changes to JET and its divertor since the PTE, the neutron yield in pure deuterium, Y_{DD} , has continued to scale strongly with stored diamagnetic energy, W_{dia} , with roughly constant reactivity, Y_{DD}/W_{dia}^2 . This scaling covers the dependence of the neutron yield on the squares of the thermal and fast particle energies and their product as expected from thermonuclear, beam-beam and beam-plasma reactions, and variations in the reactivity will arise from variations in profiles, T_i , T_i/T_e , Z_{eff} and beam energy. It is clear therefore that these parameters have not varied significantly in this regime.

D-T simulations using TRANSP have been made for a number of such pulses, assuming transport coefficients deduced from the D-D pulses, i.e. neglecting isotopic effects, but including alpha particle heating. These simulations, which will be described in more detail in [16], also show a quadratic dependence between the predicted D-T fusion powers and diamagnetic stored energies (Fig. 2). It is important to point out that these simulations suggest a fusion power multiplication factor of 210, consistent with the profile weighted ratio of the fusion cross sections [17]. Figure 2 contains simulated fusion power versus simulated W_{dia} and 210 times the measured D-D fusion power, P_{DD} , versus measured W_{dia} . The two curves correspond to a quadratic dependence of $210 \times P_{DD}$ with W_{dia} , the first an upper bound of all the D-D data and the second a typical curve through the combined NB and ICRF heating data (although the bulk of this data is omitted for clarity). A large part of the scatter in predictions between the two curves indicate systematic variations in reactivity due to variations in T_i/T_e , Z_{eff} and fast ion energy content. In particular, low power NB-only and high power combined heating tend to cluster about the lower curve, whereas high power NB-only data tend towards the upper curve. The TRANSP simulations introduce additional scatter as a result of uncertainties in the kinetic measurements. Nevertheless, there is a clear strong improvement of expected performance with increasing stored energy which provides a useful benchmark for the D-T measurements to be presented later.

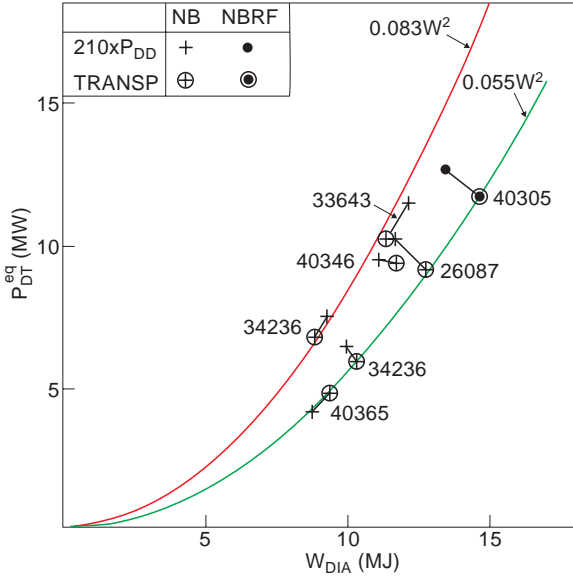


FIG. 2. Equivalent D-T fusion power P_{DT}^{eq} from D-T simulations based on D-D discharges using TRANSP (see text) against simulated stored diamagnetic energy (circled symbols). The plain symbols are 210 times the measured D-D fusion power at the measured diamagnetic energy. The two curves are both $P_{DT}^{eq} \propto W_{dia}^2$; the upper curve delineates the upper bound of $210 \times P_{DD}$ for all ELM-free data in the period 1991-1997, and the lower curve delineates the typical trend of $210 \times P_{DD}$ for combined heating data in D-D for the Mark II divertor only.

to know the relative contributions to the neutron rate from beam-plasma reactions due to deuterium on tritium and tritium on deuterium, and from thermonuclear reactions. These were estimated from TRANSP extrapolations from a pure deuterium discharge to D-T. The TRANSP results were then scaled for different NB mixes by a simple model which assumed that the recycling contribution of deuterium was proportional to the total NB particle flux (deuterium and tritium), with the constant of proportionality, f , to be determined experimentally. If recycling could be neglected ($f=0$), the peak fusion yield would occur with a NB mix of 45% tritium (weighted towards deuterium rich by the tritium on deuterium beam-plasma reactions). However, the maximum fusion yield was found experimentally with 100% tritium NB injection, and the experimental dependence of fusion power with NB mix indicated $f=2$, i.e that recycling dominated the plasma mix. TRANSP analysis of this experiment qualitatively confirms the result of the simple model [19]. This experiment clearly demonstrated that it would be necessary to replace deuterium gas fuelling by mixed D-T fuelling and to load the walls with an appropriate D-T mix for the high power experiments.

3.2. Mixture Control in D-T

The PTE experiments with 11% tritium injected by NB suggested [12] that the plasma mix reflected the NB mix, indicating that either recycling was negligible (because the particle confinement was so good) or the injected species was reflected at the walls (rather than deuterium being desorbed). However, an experiment with the Mark II divertor with selective hydrogen loading of plasma facing surfaces suggested that the dilution of core fuelled deuterium discharges could be significant even under conditions of low recycling [18]. To clarify the relative contributions of NB fuelling and recycling to the plasma mix in the ELM-free H-mode regime, the NB mix was varied from pure deuterium to pure tritium whilst the walls were still predominantly deuterium and the D-T neutron rate was measured. Such a variation in NB mix was possible with 10 MW of injected NB power by selecting appropriate beams from each of the two NB injectors. To interpret the results of this experiment it is only necessary

3.3. High Power Pulses in D-T

In all, eight high power ELM-free pulses were produced, as listed in Table I. The first, which used D-T mixtures for both gas and NB fuelling whilst the walls were still predominantly deuterium, confirmed the conclusions of the mixture control experiment at higher NB particle fluxes. For the remaining experiments, the walls were loaded using 3-5 ohmic or ICRF heated pulses with the gas fuelling adjusted until the measured D-T plasma mix was close to 50:50. The target density and pre-programmed gas flows were adjusted in 1 to 2 short (<0.5 s) high power pulses. Finally, the full duration pulse was selected.

Table I Maximum values for the eight high power ELM-free H-mode pulses in D-T

Pulse No.	42665	42675	42676	42677	42968	42974	42976	42979
Comment	walls deuterium	sawtooth limited	NB+ ω_{cH}	NB only	NB+ ω_{cH} +2 ω_{cT}	NB+ ω_{cH}		early switch off
Time (s)	13.14	13.15	13.34	13.3	13.25	13.37	13.4	13.0
I_p (MA)	3.7	3.65	3.64	3.62	3.99	3.98	3.95	4.03
B_T (T)	3.4	3.4	3.4	3.4	3.6	3.6	3.6	3.6
P_{NB} (MW)	18.3	18.7	18.8	21.3	18.7	22.3	22.3	20.3
P_{RF} (MW)	2.7	3.6	3.6	0	5.4	3.0	3.1	3.1
P_{in} (MW)	21.3	23.2	22.6	21.6	25.1	25.6	25.7	23.8
P_{DT} (MW)	8.7	10.0	12.9	12.3	12.4	15.8	16.1	10.7
W_{dia} (MJ)	12.3	13.2	15.3	13.4	15.8	16.9	17.0	13.4
$n_T/(n_T+n_D)$	0.26	0.52	0.54	0.49	0.62	0.67	0.59	0.63
$Q_{in}=P_{DT}/P_{in}$	0.40	0.43	0.57	0.57	0.51	0.64	0.62	0.45
Q^{ptot}	0.7		0.70	0.77		0.95	0.95	

Notes: I_p is the plasma current, B_T is the toroidal field at $R=3m$. P_{NB} , P_{RF} and P_{in} are the power inputs to the torus from NB, ICRF and total, including ohmic. P_{DT} is the total fusion power as measured by the total neutron yield. W_{dia} is the diamagnetic stored plasma energy. $n_T/(n_T+n_D)$ is the fraction of tritium as measured by the neutral particle analyser. The quoted Q^{ptot} values have an uncertainty of $\pm 18\%$.

The first series of experiments was performed with the standard 3.8 MA / 3.4 T scenario as developed in deuterium (including the same 0.4 MA/s current ramp-down to stabilise outer modes) in order to permit a direct comparison between D-D and D-T for both NB-only and NB supplemented by 3 MW of fundamental hydrogen minority ICRF heating. The NB-only case produced 12.3 MW of fusion power for 21.3 MW of NB power, compared with a projected 9.2 MW fusion power for 19.1 MW of NB power from simulations based on the equivalent (but lower power) D-D discharge. With combined heating, 12.9 MW of fusion power was produced

with 22.4 MW of additional heating power, compared with a projected 12.2 MW for 22.0 MW input. The uncertainty in these measurements arising from the accuracy of the neutron measurements is $\pm 8\%$, so this fusion power clearly exceeded the previous record [4].

The second series of experiments was carried out at a higher toroidal field and plasma current (4.2 MA / 3.6 T) and took full advantage of the higher NB power available in tritium. Mixed hydrogen minority and second harmonic tritium ICRF heating was also tested [20], producing 12.4 MW of fusion power for a total heating power of 25.1 MW, the additional RF power providing only electron heating. A new record D-T fusion power, 16.1 MW, was obtained with a total heating power of 25.4 MW which included NB heating (22.3 MW) together with hydrogen minority ICRF heating (3.1 MW).

The maximum value of the ratio of $Q_{in}=P_{DT}/P_{in}$ for these high power pulses is shown in Table I to vary from 0.40 to 0.64, reflecting differences in fuel mix, Z_{eff} , confinement and duration of the high performance phase. In comparison with the highest fusion power discharge in TFTR with $Q_{in}=0.27$ [4], the JET discharges produced higher fusion power for lower input power to the torus.

Some time traces for the best JET pulse are shown in Fig. 3. In common with the D-D experience, stored energy, fusion power and electron density rise monotonically with time. The ion temperature levels off around 28 keV, significantly higher than the electron temperature which is about 14 keV. The discharge does not reach steady conditions, but is limited by MHD activity: first an outer mode, then a giant ELM (as described previously for deuterium plasmas).

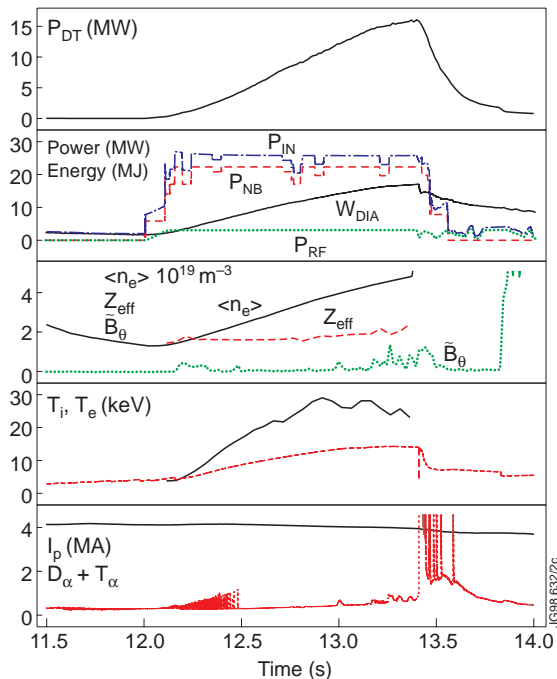


FIG. 3. Various time traces for the D-T pulse with highest fusion power. Note that following the ELM the density rises to $\sim 8 \times 10^{19} \text{ m}^{-3}$ and remains off scale.

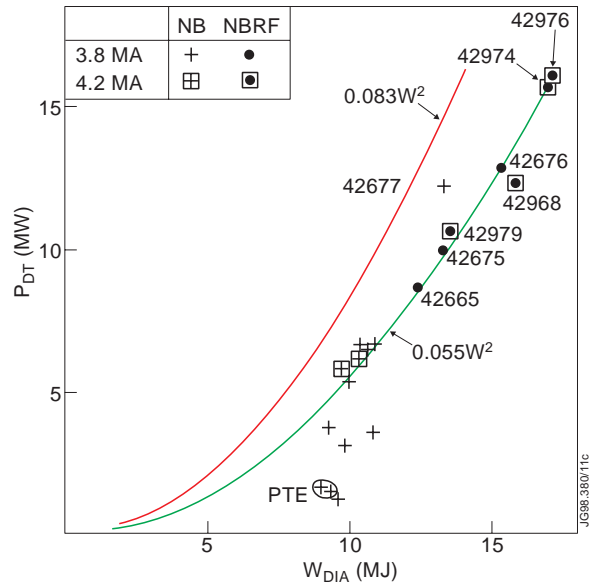


FIG. 4. Measured D-T fusion power for all ELM-free plasmas in D-T against measured diamagnetic energy. The two points labelled PTE are from the Preliminary Tritium Experiment. The curves through the data are the same as in Fig. 2.

This MHD activity manifests itself in the intensity of the Balmer alpha emission and, following detection of a giant ELM, the heating power is switched off to limit the total neutron production. In D-D, with the heating maintained, such discharges evolved into a repetitive ELMy behaviour with lower fusion performance. A more detailed comparison of the MHD behaviour in D-D and D-T plasmas will be presented in [21].

Figure 4 shows the measured D-T fusion power as a function of diamagnetic stored energy which can be compared with the D-T projections of Fig. 2. Neutral beam heating only, combined heating (NBRF) and the higher current data are distinguished by different symbols. The low power mixture control experiments together with the data from the alpha particle heating experiment (Section 4) are also included, as are the two 11% tritium pulses from the PTE. The low power experiments clearly find an optimum reactivity and these data, taken with those at high power, are well described by $P_{DT} \propto W_{dia}^2$, indicating good mixture optimisation and high reactivity throughout the series, independent of power and plasma current. The high power NB only data is a little above the curve through the combined heating data as tends to be the case in D-D (Fig. 2). The improved fusion performance at higher plasma current is a result of the higher stored energy; the 17 MJ attained is higher than achieved previously on JET or any other magnetic plasma confinement experiment.

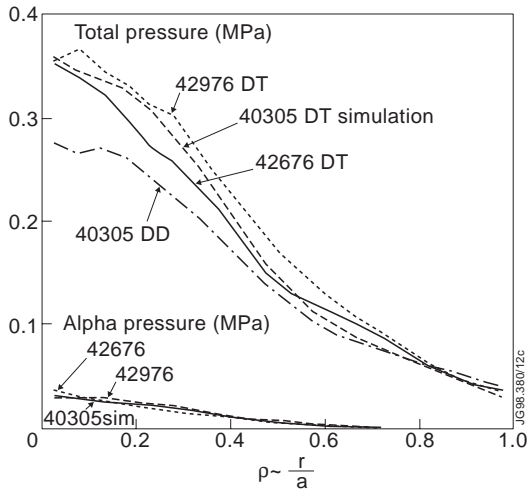


FIG. 5. Profiles of total pressure computed by TRANSP for D-D pulse No. 40305, the D-T simulation based on pulse No. 40305, the D-T pulse No. 42676 at the same plasma current (3.8 MA) and heating power, and the highest fusion power pulse No. 42976 (at 4.2 MA). The D-T pulse at 3.8 MA is intermediate between the D-D case and the D-T simulation.

3.4. TRANSP Analysis of the D-T Pulses

Figure 6 shows that there is excellent agreement between directly measured quantities and those computed by TRANSP. In particular, the measured diamagnetic energy is in excellent agreement with that computed by TRANSP, $W_{dia} = W_{th} + 3/2 W_{\perp tot}^f$, where W_{th} is the kinetic

Comparing the NB-only and NBRF data in Figs. 2 and 4, the ratio of the fusion power in D-T to that in D-D is within $\pm 10\%$ of the expected ratio of 210 at the same stored energy, in contrast to the results obtained on TFTR [4]. Figure 5 shows that the shape of the total pressure profile in D-T is similar to that in D-D and, within experimental uncertainties, is close to that projected for D-T. In fact, the difference between the D-D and D-T profiles reflects the population of energetic alpha particles produced by the fusion reactions. On the face of it, these observations confirm the assumption used in the extrapolations to D-T that the net isotope effect on energy confinement is negligible.

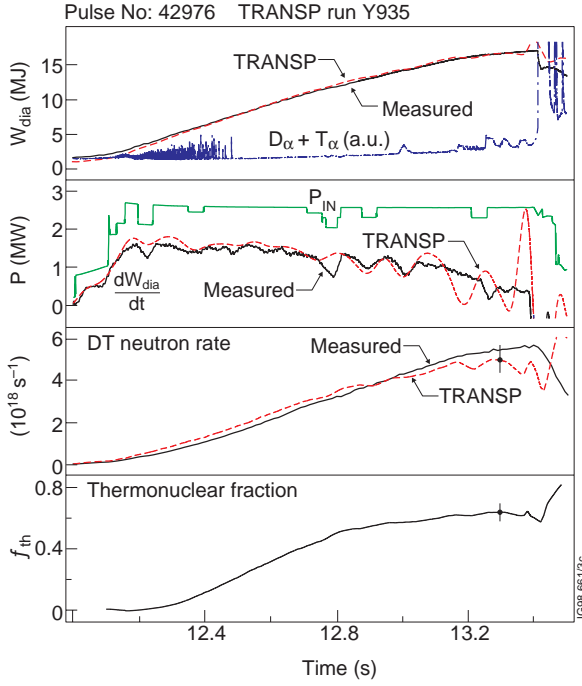


FIG. 6. Validation of TRANSP analysis and kinetic data for pulse No. 42976 by reference to direct measurements of diamagnetic energy, W_{dia} , derivative dW_{dia}/dt and neutron rate. The bottom panel shows the thermonuclear fraction.

50 ms in order to minimise statistical noise. With such smoothing there is reasonable agreement between measured and computed dW_{dia}/dt over most of the pulse, even during fluctuations in Z_{eff} (in magnitude comparable to the error estimates) which contribute to fluctuations in the kinetic measurement of dW_{th}/dt . For this reason the derivative of the thermal energy is computed from $dW_{th}/dt = d(W_{dia} - 3/2 W_{\perp tot}^f)/dt$ because the fast particle energy is almost constant. A TRANSP run (Y936) has been performed with these Z_{eff} fluctuations removed, and this improves the agreement between measured and computed quantities and yet has a negligible (<5%) effect on the power balance. It is therefore concluded that the TRANSP run (Y935) using only measured data provides an adequate description of the behaviour of fast ions and the thermal plasma.

Figure 6 also shows the thermonuclear fraction (the ratio of thermonuclear power to total fusion power, $f_{th} = P_{DT}^{th}/P_{DT}$) as computed by TRANSP, which reaches a value of about 0.63. In order to estimate the uncertainty in the thermonuclear fraction it is valid, given the small uncertainty in the measured neutron rate, to constrain the computation to match the measured neutron rate exactly. This gives an uncertainty in f_{th} of ± 0.05 relative to the reference TRANSP run.

The measured and computed data for pulse No. 42976 which produced the highest fusion power, are summarised in Table II at a time (13.13 s) when the plasma is still quiescent. The first point to note is the global power balance, which shows that of the total power input to the torus ($P_{in} = 25.7$ MW), the total power from external sources absorbed by the thermal plasma is

measurement of the thermal energy content and $W_{\perp tot}^f$ is the computed total perpendicular fast ion energy. It should be noted that TRANSP (run Y935) computes the neutron yield directly from the kinetic measurements. The error bar on this computation reflects the uncertainties in $T_i(r)$ and $Z_{eff}(r)$ assuming that these are the dominant uncertainties. The agreement is satisfying, indicating not only the quality of the measurements but also that TRANSP contains the appropriate physics.

The measured derivative of the diamagnetic energy has a resolution which can be as short as 1 ms and resolves the effect of NB interrupts and MHD events as can be seen by comparing with the traces P_{in} and $D_{\alpha} + T_{\alpha}$. With a TRANSP time step of 10 ms and 2000 particles in the Monte Carlo NB slowing down calculation it is necessary to smooth over 30-

Parameter	Values at 13.13 s	Max. Values	Units
Plasma current, I_p	4.02	4.18	MA
Toroidal field, B_T	3.6		T
NB power, P_{NB}	22.3		MW
RF power, P_{RF}	3.1		MW
Total power input to torus, P_{in}	25.7		MW
Absorbed external power, P_{abs}^{th}	21.9		MW
Total thermal heating power, $P_{heat}^{th} = P_{abs}^{th} + P_{\alpha abs}^{tot}$	23.5		MW
Loss power, $P_{loss}^{th} = P_{heat}^{th} - dW_{th}/dt$	13.2	19 before ELM	MW
Electron density, n_e	4.1		$10^{19} m^{-3}$
Fuel density, $n_D + n_T$	3.3 ± 0.3		$10^{19} m^{-3}$
Mean Z_{eff}	1.9 ± 0.2		
Central ion temperature, $T_i(0)$	28 ± 2		keV
Central electron temperature, $T_e(0)$	14		keV
W_{th}, W_{dia}	12.0, 15.5	13.6, 17.0	MJ
$dW_{th}/dt, dW_{dia}/dt$	10.3, 10.2		MW
τ_E thermal, diamagnetic	0.90, 0.94		s
$(n_D + n_T) T_i(0) \tau_E$ thermal, dia	8.3, $8.7 \pm 20\%$		$10^{20} m^{-3} keVs$
$(n_D + n_T)/n_e$, TRANSP	0.80		
$n_T/(n_D + n_T)$: NPA, TRANSP	0.59, 0.49		
Neutron rate	5.0	5.7	$10^{18} s^{-1}$
DT fusion power, P_{DT}	14.2	16.1	MW
DT fusion energy		13.8	MJ
Alpha particle source power, P_{α}^s heating, $P_{\alpha abs}^{tot}$	2.83, 1.62	3.15, 2.52	MW
$Q_{in} = P_{DT}/P_{in}$	0.55	0.62	
P_{DT}/P_{abs}	0.60	0.74	
Q_{th}^p	0.69 ± 0.19		
Q_{tot}^p	0.95 ± 0.17		
Thermonuclear fraction, f_{th}	0.61 ± 0.05	0.63	
$P_{\alpha}^s/P_{loss}^{tot}, P_{\alpha abs}^{tot}/P_{loss}^{th}$	0.17, 0.12		

Table II Parameters of interest for ELM-free H-mode pulse No. 42976 with the highest D-T fusion power, at the time of maximum Q_{tot}^p (13.13 s) and maximum value of each parameter, if significantly different. The geometric parameters of this pulse are: minor radius $a = 0.95m$, major radius $R = 2.92m$, $q_{95} = 3.47$, elongation $\kappa = 1.81$, triangularity $\delta = 0.36$. The divertor plasma is attached. Computed quantities are from TRANSP run Y935.

$P_{\text{abs}}^{\text{th}}=21.9$ MW (including direct heating, fast particle heating and thermalisation, and the heating by rotation friction). The difference (3.6 MW) includes losses due to NB shine-through, fast particle charge exchange and rotation (but excluding frictional heating). An alpha particle source power, $P_{\alpha}^{\text{S}}=2.83$ MW is measured from the D-T fusion neutron rate, and, taking into account the alpha particle slowing down, an alpha particle heating power $P_{\alpha \text{ abs}}^{\text{tot}}=1.62$ MW is computed to be absorbed by the thermal plasma. The total heating power transferred to the thermal plasma from all sources is therefore $P_{\text{heat}}^{\text{th}}=23.5$ MW. The rate of change of plasma thermal energy dW_{th}/dt is large, and the thermal loss due to conduction, convection, radiation and thermal charge exchange is $P_{\text{loss}}^{\text{th}}=P_{\text{heat}}^{\text{th}} - dW_{\text{th}}/dt=13.2$ MW. The total loss from the plasma including thermal, rotational and fast ion loss channels (but excluding NB shine-through) is $P_{\text{loss}}^{\text{tot}}=16.2$ MW. A time dependent power balance is shown in the top panel of Fig. 7, and this is used to compute the confinement time¹ in the lower panel. The value of $n_{\text{DT}}(0)\tau_{\text{E}}T_{\text{i}}(0)$ is 8.3 or $8.7 \times 10^{20} \text{ m}^{-3} \text{ skeV}$ ($\pm 20\%$), depending on whether the thermal or diamagnetic energy confinement time ($\tau_{\text{E}}^{\text{th}}$, $\tau_{\text{E}}^{\text{dia}}$) is used (see Table II for values of $n_{\text{DT}}(0)$, $\tau_{\text{E}}^{\text{th}}$, $\tau_{\text{E}}^{\text{dia}}$ and $T_{\text{i}}(0)$).

The central fusion power density, 0.63 MW/m^3 , exceeds the central power density absorbed from external sources, 0.59 MW/m^3 , and does so out to 35% of the minor radius. The alpha particle source power density is about 0.12 MW/m^3 at the centre and the alpha particle

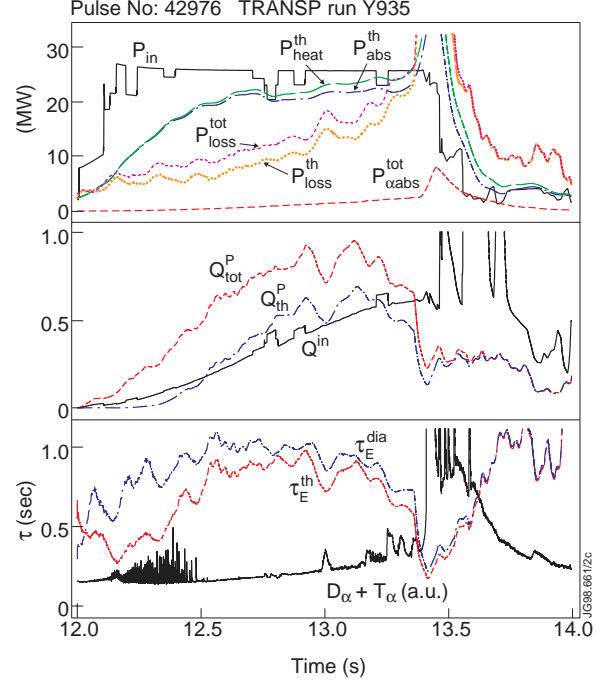


FIG. 7. Time dependent performance analysis for pulse No. 42976. The top panel shows the global power balance including the total power input to the torus $P_{\text{in}}=P_{\text{OH}}+P_{\text{NB}}+P_{\text{RF}}$, the total power, $P_{\text{abs}}^{\text{th}}$, from external sources absorbed by the thermal plasma, the alpha particle power transferred to the thermal plasma $P_{\alpha \text{ abs}}^{\text{tot}}$ and the total heating power to the thermal plasma $P_{\text{heat}}^{\text{th}} = P_{\text{abs}}^{\text{th}} + P_{\alpha \text{ abs}}^{\text{tot}}$. The power escaping from the thermal plasma, $P_{\text{loss}}^{\text{th}}$, and the total loss power in all channels, $P_{\text{loss}}^{\text{tot}} = P_{\text{loss}}^{\text{th}} + P_{\text{loss}}^{\text{rot}} + P_{\text{loss}}^{\text{fast}}$, are shown. The bottom panel shows the diamagnetic and thermal energy confinement times, $\tau_{\text{E}}^{\text{dia}}$ and $\tau_{\text{E}}^{\text{th}}$, and the Balmer α signal. The middle panel compares the simple ratio, $Q_{\text{in}}=P_{\text{DT}}/P_{\text{in}}$ with thermal, Q_{th}^{P} , and total, $Q_{\text{tot}}^{\text{P}}$, as defined in the text.

¹ The thermal energy confinement time is defined as $\tau_{\text{E}}^{\text{th}}=W_{\text{th}}/P_{\text{loss}}^{\text{th}}$, and the diamagnetic energy confinement time as $\tau_{\text{E}}^{\text{dia}}=W_{\text{dia}}/(P_{\text{in}}+P_{\alpha}^{\text{S}}-P_{\text{SH}}-P_{\text{BCX}}-dW_{\text{dia}}/dt)$. W_{th} , W_{dia} , $P_{\text{loss}}^{\text{th}}$, P_{in} and P_{α}^{S} are defined in the text. In addition P_{SH} is the NB shinethrough power and P_{BCX} is the net NB power lost from NB fast ions by charge exchange on the background neutrals.

heating power density (including orbit effects and slowing down) is about 0.06 MW/m^3 most of which is coupled to electrons. The central alpha particle heating of electrons is comparable to each of the centrally absorbed powers (from external sources) to the electrons, equipartition from ions to electrons and the change in electron energy density which are of comparable magnitude. The alpha particle heating should therefore be significant and this is examined in Section 4.

3.5. D-T Fusion Performance Parameters

A value of $n_{DT}(0) \tau_E^{\text{th}} T_i(0) \approx 9 \times 10^{20} \text{ m}^{-3} \text{ s keV}$ (at the same $T_i(0)$, pressure profile peaking and relative ion and electron temperatures as pulse No. 42976) would, for a pure thermonuclear plasma, correspond to $Q = P_{DT}/(P_{\text{loss}} - P_{\alpha}) \approx 1$ and $P_{\alpha}^S/P_{\text{loss}} \approx 16\%$. If the same conditions could be maintained into steady-state, $P_{\text{in}} = P_{\text{loss}} - P_{\alpha}$, and therefore $Q_{\text{in}} = P_{DT}/P_{\text{in}}$ would also approach unity.

In reference [1] a definition of Q was chosen in such a way as to indicate, for a NB heated plasma, the likely stationary value of P_{DT}/P_{in} which would be obtained were it possible to maintain the same plasma parameters by reducing the input power by the amount of the derivative of stored energy. Following this approach would suggest that the steady-state equivalent of pulse No. 42976 would correspond to $P_{DT}/(P_{\text{in}} - P_{\text{SH}} - P_{\text{BCX}})$ in the range 0.8-0.9 [22], approximately commensurate with the observed values of $n_{DT}(0) \tau_E^{\text{dia}} T_i(0)$. However, this treatment neglects the finite slowing down time of the alpha particles, the RF driven fast particles, and the small but non-negligible effect of rotation in the power balance. In the following paragraphs two new parameters, Q_{th}^P and Q_{tot}^P , are defined, which rigorously include all terms in the power balance and can be applied to both transient and steady-state plasmas.

Firstly, it is proposed to define a parameter Q_{th}^P to describe the thermonuclear performance of plasmas in terms of losses from the thermal plasma:

$$Q_{\text{th}}^P = P_{\text{th}} / (P_{\text{loss}}^{\text{th}} - P_{\alpha \text{ abs}}^{\text{th}})$$

which can be applied to both transient and stationary cases. $P_{\text{th}} = f_{\text{th}} P_{DT}$ is the thermonuclear power, $P_{\text{loss}}^{\text{th}}$ is the power escaping from the thermal plasma and $P_{\alpha \text{ abs}}^{\text{th}}$ is the alpha particle heating power transferred to the thermal plasma from thermonuclear reactions. In fact, this definition differs from that used in [1] only in that it takes account of the alpha particle slowing down. Q_{th}^P is then a function of $(\tau_E^{\text{th}})^2 \times P_{\text{loss}}^{\text{th}}$ and the reactivity $P_{\text{th}}/W_{\text{th}}^2$, even for transient conditions, and encapsulates the underlying physics of confinement and thermal profiles. Of course Q_{th}^P does not necessarily remain constant as stationary conditions are approached unless $(\tau_E^{\text{th}})^2 \times P_{\text{loss}}^{\text{th}}$ remains constant.

Secondly, it is proposed to define a parameter Q_{tot}^P which describes the total fusion performance in terms of all losses from the plasma:

$$Q_{\text{tot}}^P = P_{DT} / (P_{\text{loss}}^{\text{th}} + P_{\text{loss}}^{\text{rot}} + P_{\text{loss}}^{\text{fast}} - P_{\alpha \text{ abs}}^{\text{tot}})$$

and deals consistently with the more complex situation where the power lost from the plasma now also includes rotation, $P_{\text{loss}}^{\text{rot}}$, and NB/RF fast particle losses, $P_{\text{loss}}^{\text{fast}}$ (such as charge-exchange and orbit losses). $P_{\alpha \text{ abs}}^{\text{tot}}$ is the total heating by alpha particles from both thermonuclear and non-thermal reactions taking account of the slowing down of the alpha particles. The losses in this expression can be computed from the TRANSP power balance,² provided that the derivatives can be computed accurately as was demonstrated in Section 3.4.

A fairly comprehensive picture of the time dependent performance can be obtained by comparing Q_{in} , $Q_{\text{tot}}^{\text{P}}$ and Q_{th}^{P} , as shown in Fig. 7 (second panel). Whereas Q_{in} increases monotonically up to the ELM (to a maximum of 0.62), both $Q_{\text{tot}}^{\text{P}}$ and Q_{th}^{P} rise rapidly over the first 0.8 s and remain approximately constant for 0.4-0.5 s indicating that, though fusion and loss powers are changing rapidly with time, they are doing so in proportion. The peak values $Q_{\text{tot}}^{\text{P}} = 0.95 \pm 0.17$ and $Q_{\text{th}}^{\text{P}} = 0.69 \pm 0.19$ are broadly in line with expectations based on the corresponding values of $n_{\text{DT}}(0)\tau_{\text{E}}T_{\text{i}}(0)$.

Note that there is a degradation in these performance indicators with the MHD burst from around 13.2 s (before the ELM) which is also seen on the confinement time (lowest panel in Fig. 7). However, Q_{in} continues to increase up to the time of the ELM, suggesting that the MHD activity increases the losses with little effect on the reactivity of the plasma. At the ELM there is a significant rise in density and fall in electron temperature. The consequent change in slowing down transiently increases the alpha particle heating power to ≈ 8 MW and the total thermal heating power to ≈ 44 MW (off scale). The drop in $Q_{\text{tot}}^{\text{P}}$ accurately reflects the reduction in performance during this phase whilst the high value of Q_{in} clearly has no meaning.

The performance parameters $Q_{\text{tot}}^{\text{P}}$ and Q_{th}^{P} permit a more detailed comparison of the eight pulses shown in Table I. In particular, these parameters can be used to identify the effect of

²The denominator in this equation for $Q_{\text{tot}}^{\text{P}}$ can be computed from the power balance:

$$P_{\text{loss}}^{\text{th}} + P_{\text{loss}}^{\text{rot}} + P_{\text{loss}}^{\text{fast}} - P_{\alpha \text{ abs}}^{\text{tot}} = P_{\text{OH}} + P_{\text{NB}}^{\text{S}} + P_{\text{RF}}^{\text{S}} - d(W_{\text{th}} + W_{\text{RF}}^{\text{f}} + W_{\text{NB}}^{\text{f}} + W^{\text{rot}})/dt$$

The ohmic power P_{OH} is computed by TRANSP and is very small. The NB power source P_{NB}^{S} in the plasma (i.e. NB input minus shine-through) is well known and the ICRF source power P_{RF}^{S} in the plasma due to fast particles and direct heating is computed. The derivative includes the energy stored in the thermal plasma W_{th} , in the ICRF and NB fast particles (W_{RF}^{f} and W_{NB}^{f}) and the computed rotational energy W^{rot} . It can be computed from the temporal derivative of

$$W_{\text{dia}} - 3/2 W_{\text{tot}}^{\text{f}} + W_{\text{RF}}^{\text{f}} + W_{\text{NB}}^{\text{f}} + W^{\text{rot}}.$$

The value of this derivative is dominated by W_{dia} with the fast ion corrections being small (≈ 1 MW) and is relatively independent of TRANSP assumptions, as shown by the good agreement in Fig. 6. The normal level of accuracy of the input power, neutron yield and diamagnetic stored energy are $\pm 10\%$, $\pm 8\%$ and $\pm 5\%$. If it is assumed that the errors are gaussian and that these errors dominate the computation, then the absolute uncertainty in $Q_{\text{tot}}^{\text{P}}$ is $\pm 18\%$. If it is assumed that the uncertainties in kinetic data introduce a scatter of $\pm 10\%$ in the TRANSP computation of Q_{th}^{P} , then the total uncertainty in Q_{th}^{P} is likely to be $\pm(10+18) = \pm 28\%$.

a non-optimal D-T mix, which affects Q_{th}^{P} strongly, to compare NB-only with combined NBRF and to determine the effect of plasma current. It is found that $Q_{\text{tot}}^{\text{P}}$ is the same for NB-only and NB supplemented by hydrogen minority ICRF heating, that it degrades weakly with increasing additional heating power, but improves strongly with plasma current (from ≈ 0.7 at 3.64 MA to ≈ 0.95 at 4.0 MA), as will be described in [16].

In this section a new formulation for Q has been proposed which rigorously takes into account all terms in the power balance for a plasma heated by NB injection, RF waves and alpha particles, and can be applied equally well to transient and steady-state plasmas. The three parameters Q_{th}^{P} , $Q_{\text{tot}}^{\text{P}}$ and Q_{in} provide a complete description of the performance, which is in line with the usual $n_{\text{DT}}(0)\tau_{\text{E}}T_{\text{i}}(0)$ approach. The transient values of these parameters are in accord with the expectations based on deuterium performance and as such confirm that significant progress has been made towards a tokamak reactor. From the analysis presented it is self evident that to achieve $P_{\text{DT}}/P_{\text{in}} \geq 1$ in such transient plasmas would require a significant improvement in confinement and/or reactivity. Conversely, only a relatively modest improvement in confinement and/or reactivity would be required to reach such a milestone were it possible to overcome the MHD limits which render these plasmas transient.

3.6. Stability of Alfvén Eigenmodes

Investigation of Alfvén Eigenmodes (AEs) driven by energetic particles in tokamaks is motivated by the potential for such instabilities to eject energetic fusion product alpha particles and fast particles produced by additional heating from the core of a fusion reactor, possibly leading to significant reduction of alpha particle heating and to first wall damage. The study of AEs in JET during DTE1 has demonstrated that AEs can be destabilised by the energetic ions produced by auxiliary heating [23], but no evidence of alpha particle driven AEs has been observed in the high performance discharges [24]. Similar work has been reported from TFTR [25] and JT-60 [26].

In the high performance D-T hot ion ELM-free H-mode experiments on JET with fusion powers up to 16.1 MW and central $\beta_{\alpha}(0) \leq 0.7\%$ (pulse No. 42976), no observable AE activity was found on the external magnetic measurements up to 500 kHz. Figure 8 shows spectrograms of the magnetic fluctuations in a D-D reference discharge and the highest performance D-T discharge. In the D-D reference discharge, at a toroidal magnetic field of 3.4 T, AE are excited by 4.5 MW of hydrogen minority ICRF heating (but not by 3 MW). In the D-T discharge, at 3.8 T, there is no evidence of AE excitation either by the 3 MW of ICRF heating or by the 3.2 MW of alpha particle source power. The absence of alpha particle driven AEs is in agreement with CASTOR-K stability calculations [24], where the least damped AEs ($n \approx 5$) are found to be stable due to the radial extent of the eigenmodes at high β and the additional damping provided by the high energy (≈ 160 kV) tritium NB injection.

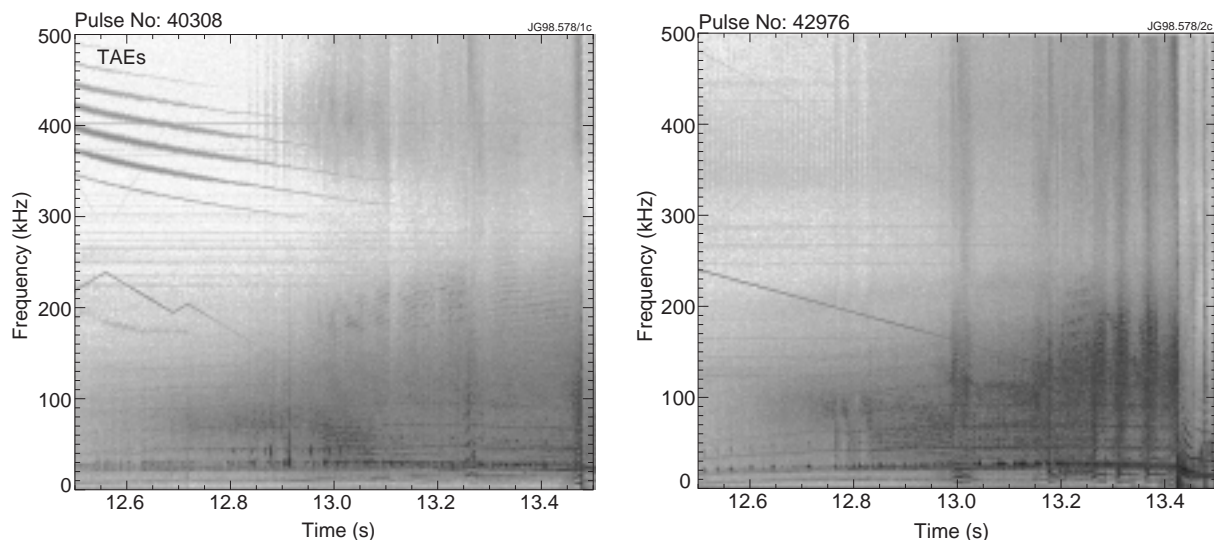


FIG. 8. Spectrograms representing the amplitude of the magnetic fluctuations measured by external Mirnov coils in (a) a D-D reference discharge (pulse No. 40308) and (b) the D-T highest fusion performance discharge (pulse No. 42976).

4. ALPHA PARTICLE HEATING

One of the original objectives of JET was the study of alpha particle production, confinement and consequent plasma heating. A wide range of experiments, reviewed in [27], has demonstrated that single fast ions in the 100keV-MeV ranges are trapped and slow-down classically in quiescent plasmas. However, fast ion losses can be caused by sawtooth crashes, toroidal field (TF) ripple or Alfvén eigenmodes (AEs). These effects are not expected to be important in the alpha particle heating experiment described here because the measurements were made just before the collapse of sawteeth which had periods (1-1.5 s) longer than the alpha particle slow-ing-down time in the plasma centre, the toroidal field ripple in JET is low, and the alpha particle pressure was not high enough to excite AEs (see Section 3.6 above). Thus, alpha particles in this experiment were expected to behave classically and, this being the case, were expected to transfer most of their energy to the plasma electrons.

The first observation of measurable alpha particle heating of the electrons in a magnetically confined plasma was made in TFTR under conditions with a fusion gain $Q_{in} = 0.27$ [28]. The hot ion ELM-free H-mode regime in JET is well-suited to the measurement of alpha particle heating since it has high current (3.8-4.2 MA) giving small alpha particle orbits, Q_{in} is about 0.6, and the alpha particle heating of electrons in the plasma core is comparable to, or greater, than each of the NB, ohmic or equipartition heating sources. The alpha particle heating is therefore important in the electron power balance and should be observable by increases in the electron temperature. The larger value of Q_{in} in JET should permit a clearer measurement of alpha particle heating than was possible in TFTR.

4.1. Design of the Alpha Particle Heating Experiment

In order to maximise the possibility of observing alpha particle heating, the discharge duration, and especially the ELM-free period, the sawtooth-free period and the electron energy confinement time, should be longer than the alpha particle slowing down time of typically 1 s. Furthermore, the electron temperature should be sufficiently high and the electron density sufficiently low for ion-electron equipartition and direct electron heating by NB heating to be low. In the JET experiments, the plasma had a central electron temperature greater than 10 keV, a central electron density less than $4 \times 10^{19} \text{ m}^{-3}$ and a total power to the electrons from these sources less than 30% of the total input power. ICRF heating was not used since it predominantly heats electrons and might be confused with the alpha particle heating.

Since experiments in other plasma regimes on other tokamaks have indicated the possibility of a plasma isotope effect on energy confinement, the JET alpha particle heating experiment [29] was designed to separate clearly any rise in electron temperature due to alpha particle heating from such an isotope effect on confinement. This was accomplished by scanning the plasma mixture from pure deuterium to nearly pure tritium. The D-T fusion power, and hence the alpha particle heating, would be maximised at intermediate concentrations of deuterium and tritium, whilst the isotopic effects could be isolated by comparing pure deuterium and nearly pure tritium plasmas.

In order to avoid temporal or spatial variations in the D-T mixture, the scan was performed using matched NB injection, gas fuelling and recycling mixtures. The last required the walls to be loaded to the required mixture using tokamak pulses between the main pulses in the scan. In this way, pulse No. 43011 with a nearly pure tritium plasma ($n_T/(n_T+n_D) \approx 92\%$) was obtained. The configuration of the NB system for DTE1 allowed a 5 point scan at a heating power of 10.4 MW, with the particle source varying between 6×10^{20} atoms/s in tritium and 8×10^{20} atoms/s in deuterium. The prototype for the experiment was the deuterium pulse No. 40365, which was a low power version of the 3.8 MA / 3.4 T high performance pulses. With 10.4 MW of NB power, a hot ion H-mode with an ELM-free period of over 2 s was obtained. This had a D-D neutron yield which projected to 4-5 MW of fusion power with a 50:50 D-T mixture. The ability to detect alpha particle heating at the 1 MW level was confirmed in a test experiment which used hydrogen minority ICRF heating as a substitute for alpha particle heating.

4.2. Measurement of Alpha Particle Heating

Pulse No. 42847, with a tritium concentration of 60%, produced the highest fusion power (6.7 MW) in the scan at an NB input power of 10.4 MW, corresponding to an absorbed power of about 9.4 MW. This is compared with the pulse (No. 43011) with a tritium concentration of 92% in Fig. 9. Just after the end of the transition ELMs, both pulses had a sawtooth before 13 s and then remained sawtooth- and ELM-free for at least 1.4 s. This allowed the central ion

temperature to reach 16-17 keV and was responsible for the better than anticipated fusion power in pulse No. 42847. Figure 9 shows that the alpha particle heating power in pulse No. 43011 is much lower than that in pulse No. 42847. Thus, the aim to have a clear peak in the alpha particle heating power, with D-T mixture, was achieved.

The effects of alpha particle heating are visible as differences in plasma thermal energy, and central ion and electron temperatures. It should be noted that the line averaged electron density is about 10% larger in pulse 43011 than in pulse 42847 at 14.2 seconds. However, the central densities are identical at $4 \times 10^{19} \text{ m}^{-3}$. Interestingly, the edge temperatures adjust so that the edge pressure is the same in both pulses and all of the difference in energy content comes from within the inner half minor radius. Whilst some of the temperature difference might, in principle, be due to the density variation, regression analysis on the full data set showed that the central electron temperature did not depend on the line averaged density.

The peak electron temperature achieved in each discharge in the scan is plotted versus time and D-T mixture in Fig. 10. Between 12.0 s and about 13.5 s alpha particle heating is small and the electron temperature is nearly independent of the D-T mixture. Later, as the fusion power becomes significant and the alpha particles have started to thermalise, the effect of alpha particle heating becomes evident. It can be seen that the maximum electron temperature increases with tritium concentration, up to 12 keV, when the concentration is 60% (pulse No. 42847), and then falls. The electron temperatures of nearly pure deuterium and tritium discharges are similar, making the identification of alpha particle heating more straightforward. The collapses of giant sawteeth are marked with squares in Fig. 10. It may be seen that the sawtooth period increases with tritium concentration. This is ascribed to an increase in the NB fast ion pressure within the $q=1$ surface [30]. In light of this variation in sawtooth period, measurements in the saturated period before the sawtooth crash have been used in the following.

The central electron temperature is shown in Fig. 11 to be proportional to the total heating power, including absorbed NB, ICRF (where appropriate), ohmic and alpha particle heating

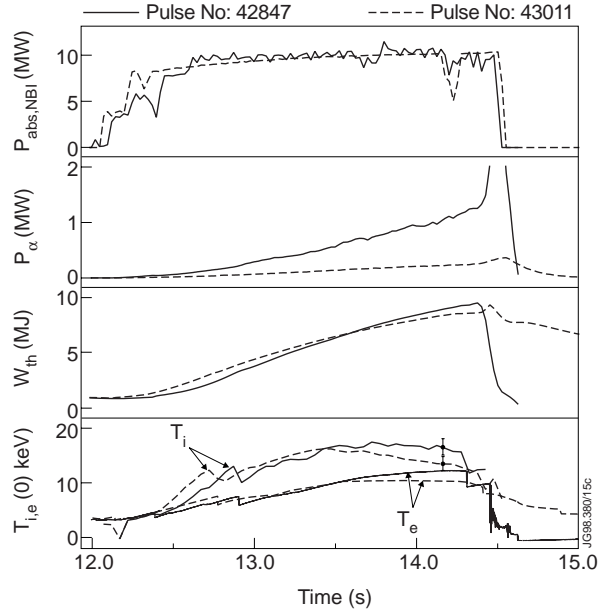


FIG. 9. A comparison of the absorbed NB heating power, alpha particle heating power, plasma energy, and ion and electron temperatures for pulses in the scan with the highest fusion power (pulse No. 42847-solid) and the highest tritium content (pulse No. 43011-dashed). The error bars shown on the ion temperature traces are the statistical errors for single time-slices. The systematic, calibration error on the electron temperature is 5%. The maximum central electron temperatures are 10.5 keV for pulse No. 43011 and 12.3 keV for pulse No. 42847.

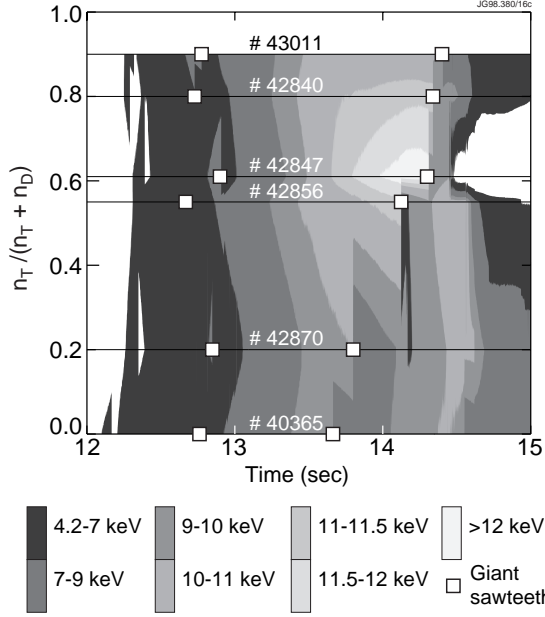


FIG. 10. Contour plot of the central electron temperature, for all the pulses in the alpha particle heating scan, against D-T mixture on the vertical axis and time on the horizontal axis. Giant sawteeth are marked by squares.

power. The variation in heating power in the D-T discharges is substantially due to the alpha particle heating (0-1.3 MW) although there is a variation in the nominal NB power, which can be as much as 10% at low tritium concentrations, as indicated by the horizontal bars. Also included in the data set are the test pulses with hydrogen minority ICRF emulating alpha particle heating. It can be seen from Fig. 11 that alpha particle heating and the ICRF heating are equally effective. This is reassuring because hydrogen minority ICRF heating is known from modulation experiments [31] to have high efficiency and a highly peaked deposition profile.

A regression fit to the data of Fig. 11 gives $T_e(0) = (0.21 \pm 0.99) + (0.99 \pm 0.09) P_{\text{heat}}^{\text{th}}$, where $P_{\text{heat}}^{\text{th}}$ is the total power absorbed by the thermal plasma, including alpha particle

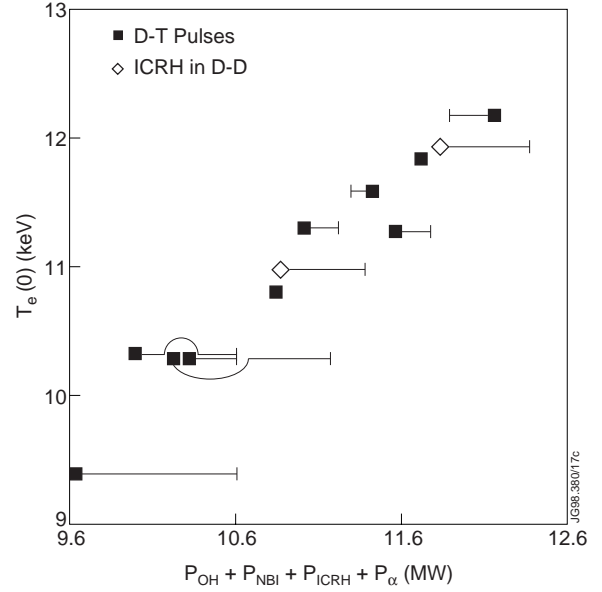


FIG. 11. The central electron temperature, just before sawtooth crashes, plotted against total absorbed heating power, including alpha particle heating power. The bars indicate deviations from the nominal value of the NB heating power of 10.5 MW. Bars to the right indicate a shortfall of power.

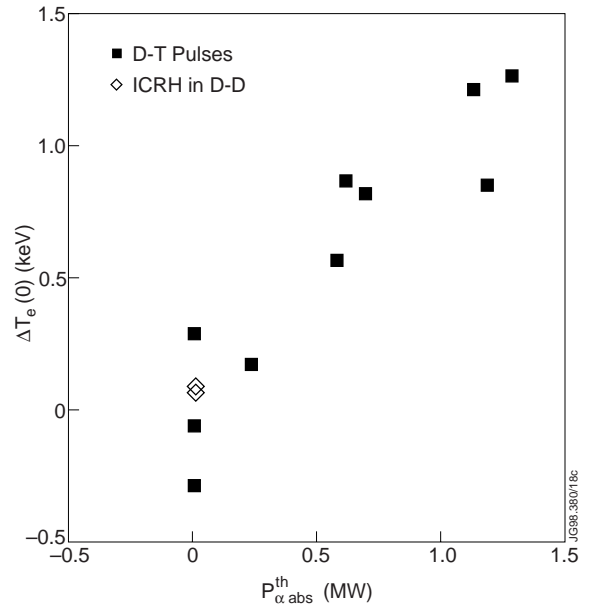


FIG. 12. The data of Fig. 11 re-plotted to show the change in electron temperature, identified by the regression fit as being due to alpha particle heating, versus alpha particle heating power.

heating. A fit which allows the contribution from the alpha particle heating to be separated from variations in the NB heating power gives $T_e(0) = (0.07 \pm 1.04) + (1.0 \pm 0.1)(P_{\text{heat}}^{\text{th}} - P_{\alpha \text{ abs}}^{\text{th}}) + (0.99 \pm 0.13)P_{\alpha \text{ abs}}^{\text{th}}$. The result is a maximum change in $T_e(0)$ of 1.3 ± 0.23 keV with 1.3 MW of alpha particle source power. If the electron density or the tritium fraction is included in the regression fit, their weights are zero within errors. This fit can be used to display the effect of alpha particle heating directly. Figure 12 shows a plot of $\Delta T_e(0) = T_e(0) - 0.07 - (P_{\text{heat}}^{\text{th}} - P_{\alpha \text{ abs}}^{\text{th}})$ versus $P_{\alpha \text{ abs}}^{\text{th}}$. This shows that once the effect of NB power variations is removed, the alpha particle heating is consistent over the scan and the standard error on the temperature change with 1.3 MW alpha particle power is a good reflection of the accuracy of the data.

4.3. TRANSP Analysis of the Power Balance

Figure 13(a) shows the electron power balance within the inner half minor radius for pulse No. 42847. The stacked curves represent sums of contributions from each term. The rate of change of energy content and the convection loss are shown inverted for clarity. The conduction loss is the difference between the upper and lower envelopes. It may be seen that the alpha particle heating is the single largest contributor to the electrons in the plasma core at 14 s, and constitutes nearly one third of the total electron source power. Furthermore, the rate of change of energy content is the largest sink, taking 1 MW out of 1.8 MW at 14 s. In contrast, in pulse No. 43011 with a tritium concentration of 92%, the rate of change of energy content is only 0.5 MW out of 1.4 MW, as shown in Fig. 13(b). The alpha particle heating is a minor part of the power balance and its absence is reflected in the rate of change of energy content. Apparently, the conduction loss is more or less the same, which seems reasonable because the plasma conditions are comparable. Note that the glitches in the traces, observable in both pulses before 13 s, are due to sawteeth.

It is important to note that the correspondence between the difference in rate of change of electron energy content and the total electron input power, within $r/a=0.5$ in the two pulses shown in Fig. 13, is a certain indication that the alpha particle heating profile is similar to that computed from the alpha particle source and classical slowing-down.

TRANSP analysis has also been used to compute the thermal energy confinement time. Within errors, the pure deuterium and nearly pure tritium pulses have the same confinement time of 1.2 s. The pulses with significant alpha particle heating have slightly higher confinement times (1.3-1.4 s), but the errors are larger. This increase in confinement time is, at least partly, due to the alpha particle heating source being more peaked than either the NB or ohmic heating. This same analysis shows that the plasma energy content is increased by 1 MJ by alpha particle heating, and that it would be more if the ELM-free period were longer.

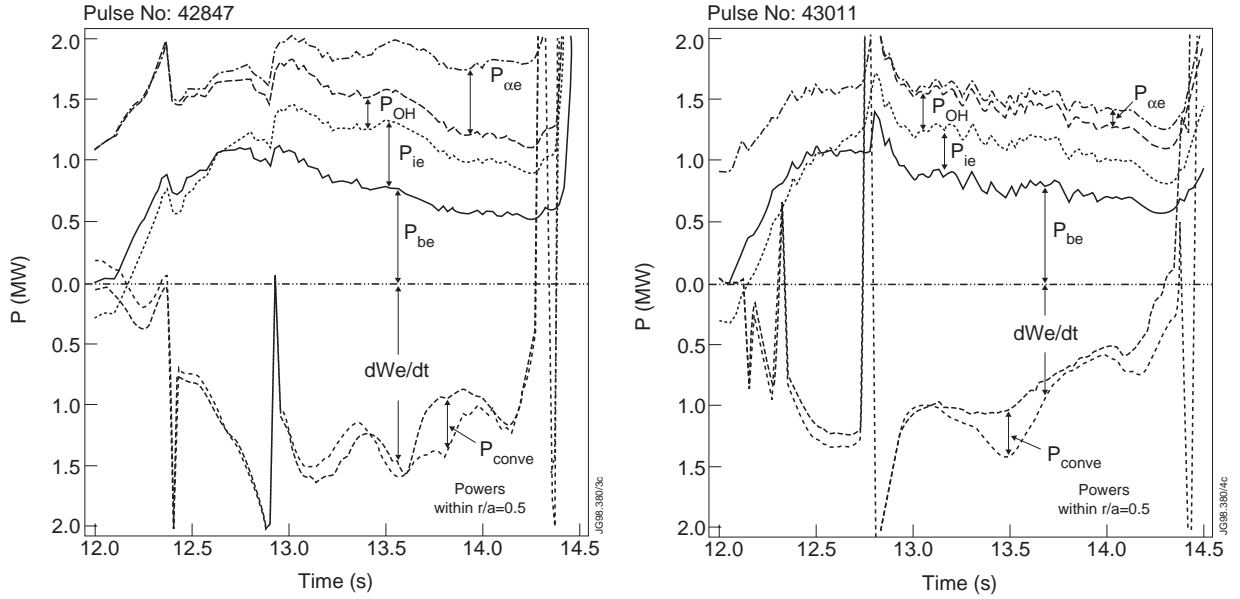


FIG. 13. The electron power balance within $r/a=0.5$ for the pulses in the alpha particle heating scan with (a) the highest fusion power (pulse No. 42847) and (b) the highest tritium content (pulse No. 43011). The rate of change of energy content and the convective loss are shown inverted for clarity.

4.4. Unambiguous Evidence for Alpha Particle Heating

The data presented above constitute unambiguous evidence for alpha particle heating because the experiment was designed to eliminate other sources of temperature change, such as any plasma isotope effect. There were clear peaks in temperature and plasma energy content as the mixture was scanned from pure deuterium to nearly pure tritium. These peaks correlate well with the alpha particle heating power as the regression analysis shows. The local electron power balances are consistent with the classical alpha particle power deposition profiles.

It should be stressed that the alpha particle heating data has been taken from MHD quiescent plasmas. Some other pulses, both from the alpha particle heating experiment and the preparation experiments for the high fusion power studies, could have been used to extend the data set but showed signs of MHD activity. This MHD activity certainly reduced the alpha particle heating, but there is no way to identify whether this is due to a loss of alpha particles or a loss of plasma confinement. A future D-T experiment should address this issue by preparing plasmas, both in D-D and D-T, with the chosen type of MHD activity, such as sawteeth, ELMs or external kink instabilities.

5. THE OPTIMISED SHEAR REGIME

The second high performance regime studied during DTE1 is the optimised shear scenario which was developed in JET to produce plasmas with energy confinement and fusion performance higher than the present ELMy H-modes. JET first obtained improved confinement of the central plasma by deep pellet fuelling of non-sawtoothed plasmas and subsequent heating of the core

[32]. The analysis of these discharges showed that the magnetic shear in the plasma centre was low and slightly negative and that the transport was reduced [33]. With negative magnetic shear, plasmas are predicted to remain stable at higher plasma pressure, and toroidal drift instabilities such as trapped particle and ion temperature instabilities are predicted to be stabilised [34]. In several experiments including JET, current profile control has allowed regimes where the heat transport is reduced significantly, close to neoclassical levels, within an Internal Transport Barrier (ITB) [34-37]. This is in line with predictive modelling [38] of such discharges, which takes into account the effect of low magnetic shear together with stabilisation by rotational shear. However, scaling laws for plasmas with ITBs have not yet been determined. In particular, the plasma isotope dependence of the threshold power for triggering an ITB has not been firmly established, although TFTR [4,6] has reported that the power needed for the formation of an ITB was much higher in D-T than in D-D.

5.1. Current Rise Scenario

The method used for optimising the current profile in JET experiments has been described in [37, 39]. The plasma current is ramped fairly rapidly, at 0.4 MA/s, so that current diffusion from the plasma edge to the plasma centre takes longer than the current ramp-up. A faster ramp-up results in strong MHD activity leading either to anomalous current diffusion or even to disruptions. Low power lower hybrid current drive, at the level of 1-2 MW, is applied promptly after the formation of the plasma to ensure a broad current profile in the early phase of the discharge and to provide strong electron heating in order to arrest current diffusion. The plasma, which is in a single null X-point configuration from the first second of the discharge, is then further pre-heated with 1-2 MW ICRF heating for several seconds before the main heating phase late in the current ramp. The ICRF frequency is such that heating (via minority species and/or at an harmonic resonance of the main ions) takes place close to the plasma centre. This combined pre-heat provides high central electron temperatures (typically 6-8 keV) and further arrests the diffusion of the current. The pre-heating phase ends with the increase of the ICRF heating power up to 6MW and the start of NB injection at powers up to 10 MW. The main heating phase starts approximately 0.4 s later combining NB and ICRF heating of typically 25 MW. It has been observed that a substantial part of the ICRF heating is damped, via the second harmonic deuterium resonance, on the NB ions or on the thermal ions when the ion pressure is sufficiently high [40,41].

5.2. Performance in D-D and Modifications for D-T

The highest fusion performance in D-D has been obtained when an H-mode transition was delayed for as long as possible. This was achieved by using a low target density, a magnetic configuration which allowed maximum pumping by the divertor cryopump, low triangularity

and by maintaining the current ramp-up throughout the main heating phase. When an ITB is established, the resulting good core confinement maintains the plasma loss power below the level required to trigger an H-mode, thus preserving a low pressure gradient at the edge, as in the L-mode. The highest fusion yield in JET D-D plasmas has been achieved in this way [40-43].

Initial experiments with tritium gas fuelling and deuterium NB injection showed that the H-mode threshold power was significantly lower in D-T than in D-D plasmas [44,45] and this was expected to be the main problem when translating the high performance obtained in D-D to D-T. In spite of this concern, it was found that ITBs can be produced in JET in D-T plasmas with similar additional heating power levels and with similar current profiles to those in D-D [46]. However, this required some developments of the current rise scenario, since the current profiles at the start of the main heating phase in D-D and D-T pulses were found to be different, as shown in Fig. 14. In D-D plasmas, the evolution of the radial location of the foot of the steep ion temperature gradient is very similar to the evolution of the radius of the $q=2$ magnetic surface as inferred using magnetic equilibrium reconstruction calculations [39-41]. Furthermore, the formation of an ITB first occurs when a $q=2$ magnetic surface appears at a small plasma radius.

In D-T plasmas, the calculated central q value was generally higher than in D-D plasmas. The difference in current profiles between D-D and D-T plasmas has not been fully understood. As shown in Fig. 14, similar q profiles can, however, be achieved in D-T by using some ^3He gas in the plasma breakdown phase, modifying slightly the plasma current ramp rate and increasing the ICRF heating power during the pre-heat phase. For the formation of the ITB a systematic analysis has also indicated a strong link between the total energy input during the pre-heating phase and the time of the L-H transition. When the pre-heating energy from both NB and ICRF heating exceeds 3MJ, an H-mode is triggered early. By using modified power waveforms, where the NB pre-heat energy is much reduced, and establishing a current profile at the onset of the high power phase such that a $q=2$ magnetic surface is present, ITBs have been produced in D-T under similar conditions to those in D-D.

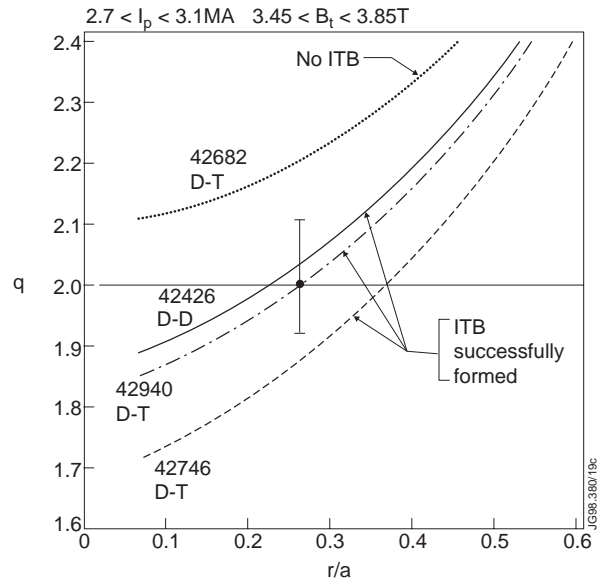


FIG. 14. q profiles from magnetic reconstruction (EFIT) at the start of the high power phase for pulses with and without production of an Internal Transport Barrier (ITB). Pulse No. 42682 in D-T is an exact repeat of D-D pulse No. 42426. Pulses Nos. 42940 and 42746 use ^3He puffs and slightly modified plasma current and ICRF heating waveforms. A typical error bar around $q = 2$ is given. The closer to the plasma centre, the larger are the error bars.

5.3. Internal Transport Barriers in D-T

The time histories of various signals for two similar D-T pulses are compared with a D-D pulse in Fig. 15. All waveforms are very similar, except for the plasma current in the high power phase which is ramped-down for D-T pulse No. 42750 and the frequency of the ICRF heating which is adjusted for hydrogen minority in D-T pulse No. 42746 and D-D pulse No. 40847 and for ^3He minority in D-T pulse No. 42750. In D-T, a sequence of events similar to those in D-D has been achieved, namely the triggering of an ITB with an L-mode edge followed by an ELM-free H-mode.

However, the time duration of the L-mode edge phase is shorter in D-T than in D-D, consistent with a lower H-mode threshold power in D-T. It is to be noted that the ramp-down in plasma current results in shortening the L-mode edge phase but increases the ELM-free H-mode edge phase. The central ion temperature rises to 35 keV (compared to 28 keV in D-D) and the fusion power reaches 8.2 MW for pulse No. 42746 as shown in Table III and Fig. 15. The initial plasma tritium concentration, $n_{\text{T}}/(n_{\text{D}}+n_{\text{T}}+n_{\text{H}})$, which has been kept low to reduce the chance of an H-mode transition, has been varied from 17% to 30% with no effect on the formation of the ITB. Figure 15 shows that the full potential of the optimised shear discharges in D-T has not yet been realised.

It has been shown [40, 41] that the density build-up within the ITB can be attributed mainly to NB fuelling during the L-mode edge phase. Recycling from the walls appears to be negligible during that phase. Therefore, the NB system has been configured to maximise the injection of tritium. The average tritium concentration in the plasma, measured by neutral particle analysis (NPA), is shown in Fig. 16 for typical optimised shear discharges in D-T. When the initial tritium content is low, the tritium concentration increases steadily but does not reach the level of the NB mix during the L-mode phase. When the ELM-free H-mode is triggered, the tritium concentration rises substantially, due to the influx of tritium from the walls. Data consistency analyses using TRANSP code simulations have indicated a tritium concentration of 29% at 6.8 s for pulse No. 42746 and of 34% at 6.2 s for pulse No. 42940, in reasonable agreement with the NPA data. It is clear from these data that the D-T mixture has not yet been optimised for

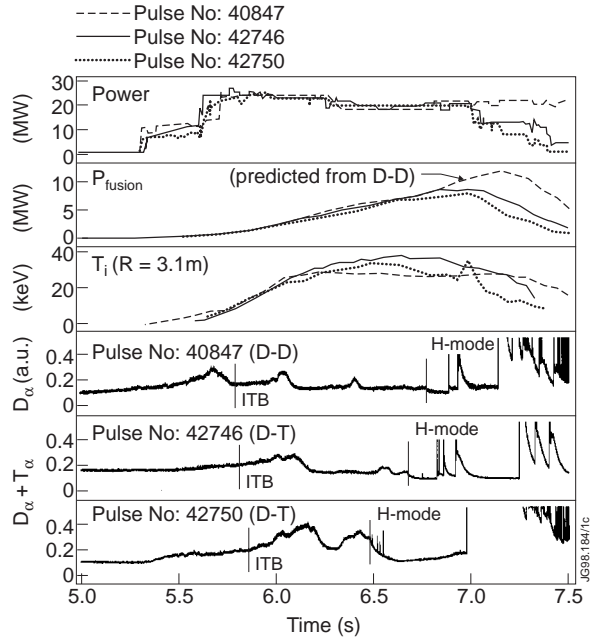


FIG. 15. Time history of typical signals for three similar pulses at $B_T=3.43 T$. I_p increases from 2.4 MA at $t = 5 s$ up to 3.25 MA at $t = 7.2 s$ for pulses Nos. 42746 and 40847. For pulse No. 42750, I_p is ramped down from 2.9 MA at $t = 6.2 s$.

Parameter	Values		Unit
	Pulse No. 42746	Pulse No. 42940	
I_p	3.2	3.3	MA
B_T	3.45	3.85	T
q_{95}	3.9	3.8	
P_{NB}	18	20	MW
P_{RF}	2.0	3.0	MW
P_{OH}	0.2	0.3	MW
P_α	1.6	1.5	MW
P_{SH}	2.6	2.9	MW
P_{CX}	0.7	0.5	MW
τ_E^{dia}	1.1	0.8	s
$n_e(0)$	3.9	4.4	$10^{19}m^{-3}$
$n_D(0) + n_T(0)$	3.2	3.4	$10^{19}m^{-3}$
$T_i(0)$	33	38	keV
$T_e(0)$	13	12.6	keV
W_{dia}	11	10	MJ
dW_{dia} / dt	9	8.4	MW
$(n_D(0) + n_T(0)) \tau_E^{dia} T_i(0)$	$11 \pm 20\%$	$10 \pm 20\%$	$10^{20} m^{-3} s keV$
$(n_D(0) + n_T(0)) / n_e(0)$	0.82	0.8	
$n_T(0) / (n_D(0) + n_T(0))$: TRANSP	0.34	0.34	
$n_T / (n_D + n_T)$ at edge: recycling light	0.14	0.2	
Neutron Rate	$2.9 \pm 10\%$	$2.6 \pm 10\%$	$10^{18} s^{-1}$
Fusion Power, P_{DT}	$8.2 \pm 10\%$	$7.3 \pm 10\%$	MW

Table III Parameters of interest for the high fusion power D-T optimised shear pulses Nos. 42746 (at 6.82 s) and 42940 (at 6.25 s).

fusion power production: the discharges are a compromise between obtaining the optimum mixture and postponing the H-mode transition.

It is to be noted that central densities in D-T plasmas are lower than in D-D. This is mainly due to a lower fuelling rate as a consequence of the need to maximise the tritium to deuterium fuelling ratio. Tritium being fuelled by the high energy NB injector (151 keV) and deuterium by the low energy NB injector (76 keV) led to higher average injected energies and lower fuelling.

In order to maintain the same total heating power, whilst maximising the tritium to deuterium fuelling ratio, the power injected by the lower energy deuterium injector (typically ≈ 76 kV) was reduced for these D-T experiments. For similar power D-D and D-T NB injection, the tritium fuelling concentration was up to 45% but the overall fuelling within the ITB was lower by at least 15%, with a comparable reduction in plasma density. As a result, the density is lower and the ion temperature is higher in D-T plasmas. The resulting central pressures at comparable times during the L-mode edge phase nevertheless reach similar values, as shown in Fig. 17. It can also be seen in Fig. 17 that the ITB is slightly narrower in D-T than in D-D, which may be due to differences in the current profiles.

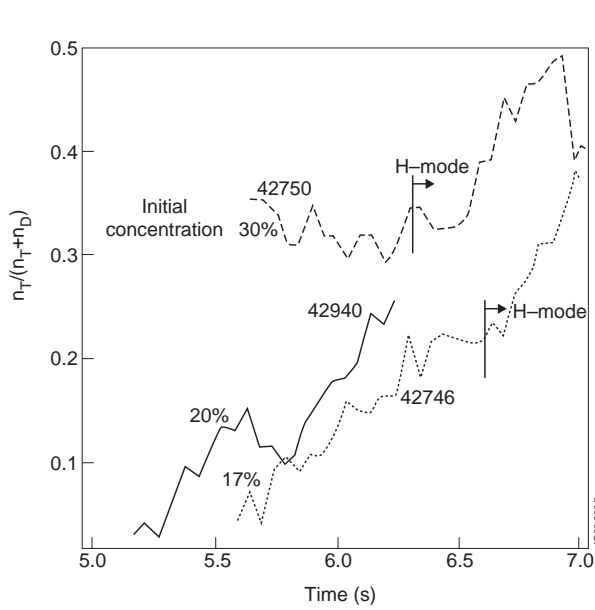


FIG. 16. Time evolution of tritium concentration for typical optimised shear D-T pulses from neutral particle analyser. The initial concentration is estimated from visible spectroscopy.

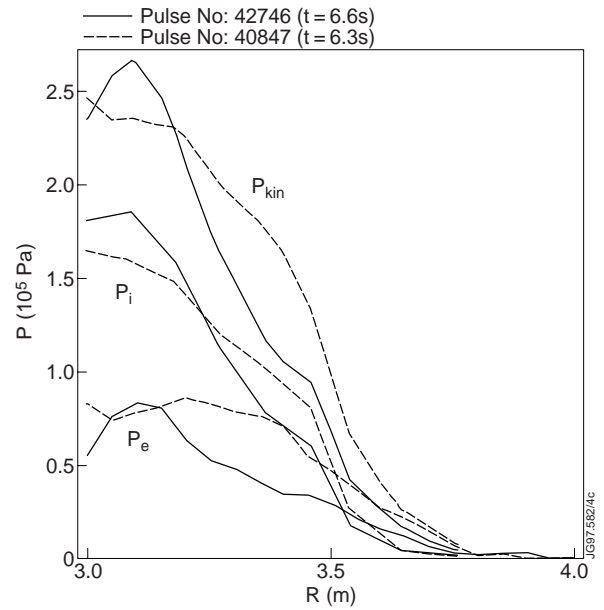


FIG. 17. Comparison of pressure profiles for two similar pulses in D-D and in D-T one second after the start of the main heating phase. The ion pressure is from charge exchange spectroscopy and the electron pressure from LIDAR measurements.

It is to be noted that the central impurity concentration in these discharges remains low, with Z_{eff} between 1.4 and 1.8, and no indication of impurity accumulation within the ITB. The concentration of the hydrogenic species $((n_D + n_T + n_H)/n_e)$ remains above 80%. These low values of Z_{eff} are attributed to the clean starting conditions and to the continuous fuelling within the ITB.

While the early part of the main heating phase leading to the triggering of an ITB has been reasonably well optimised in D-T, the limited neutron budget has prevented full optimisation of the high power phase. Such an optimisation uses real-time control of both the ICRF and NB heating powers to maximise the core pressure, whilst avoiding disruptions due to excessive plasma pressure gradients. As discussed in [47], the core pressure can be increased when the volume of the ITB expands. In D-D plasmas, this optimisation has been achieved by controlling

the power in real-time with feedback on the neutron yield. The ICRF power is normally stepped down when the neutron yield reaches a pre-set value; subsequently the NB power is controlled by a pre-set neutron yield waveform which usually increases linearly with time. In D-T plasmas, where the neutron yield depends on the D-T mix, an effective substitute for this signal has been used, consisting of the square of the diamagnetic energy multiplied by the ratio between central and edge line averaged electron density from the infra-red interferometer (representing the pressure peaking), which can be computed in real-time.

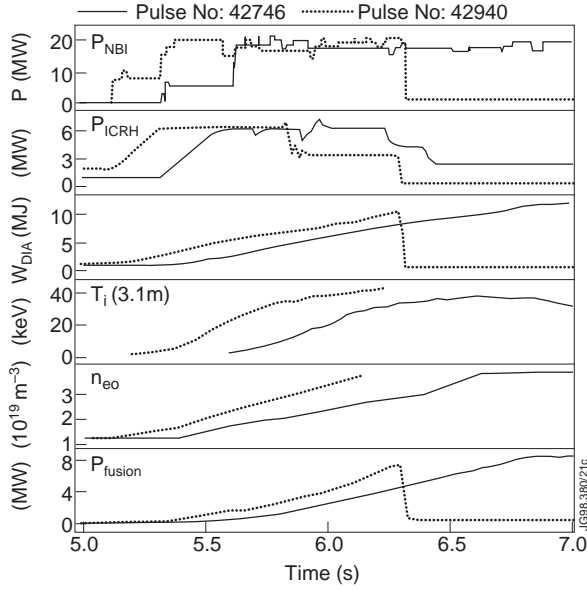


FIG. 18. Time history of typical signals for pulses Nos. 42940 and 42746 in D-T at $B_T = 3.85$ T and 3.45 T, respectively. I_p is increased from 2.6 MA at $t = 4.8$ s up to 3.3 MA at $t = 6.18$ s.

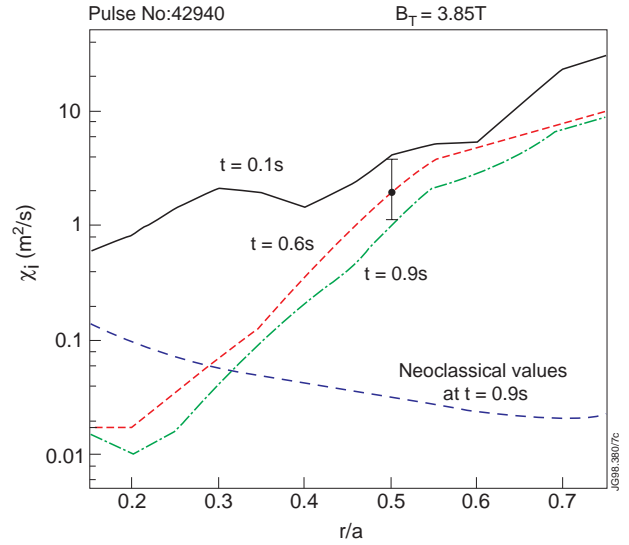


FIG. 19. Ion thermal diffusivities from TRANSP analysis for pulse No. 42940 in D-T as compared with neoclassical values. Time 0.1 s is shortly before the formation of the ITB (at 0.3 s), while the time 0.9 s is just before termination of the pulse.

Figure 18 shows the time history of typical signals for two D-T discharges at 3.45 T and 3.85 T. For pulse No. 42746, the L-H transition occurred early, limiting the fusion power to 8.2 MW. For pulse No. 42940 the demand for the neutron yield was increased but the resulting pressure gradients were too large and a disruption occurred at 6.3 s; the maximum fusion yield was 7.3 MW. The central ion temperature is very high, close to 40 keV, with ion temperature gradients of 150 keV/m, toroidal rotation speeds of 750 km s^{-1} and plasma pressure gradients of 1 MPa/m [46]. These high temperatures can be explained by the combined action of high energy NB injection and effective damping of the ICRF waves not only on hydrogen minority ions but also on deuterium ions (second harmonic) and tritium ions (third harmonic) [40,41]. TRANSP analysis shows [46] that, within the ITB, the ion thermal diffusivity decreases dramatically, approaching neoclassical [48] values in the plasma centre (Fig. 19), as in D-D plasmas. It is to be noted that the ion heat transport is lower at 3.85 T than at 3.45 T, in line with the higher ion temperature.

An important aspect of these discharges is the stability of the plasma core. An MHD stability analysis [47] indicates the need to avoid global $n = 1$ ideal pressure driven kink modes. Domains of instability are indicated in Fig. 20 for typical D-T pulses and their counterparts in D-D. The path of β_N versus peaking of the plasma pressure in D-D indicates the route for optimising the performance of such plasmas. The peaking of the plasma pressure is high when the ITB is first formed and β_N increases quickly towards the stability limit. The ITB then starts to expand after its formation and, by controlling the injected power, it is possible to increase further the plasma performance by maintaining β_N close to its limiting value. The peaking decreases substantially when the ELM-free H-mode is formed, due to the large pressure gradient at the edge. The high performance phase of the discharge is then terminated by a giant ELM. Pulse No. 42940 in D-T was not optimised and better control of the plasma pressure would have allowed substantial gains in fusion power.

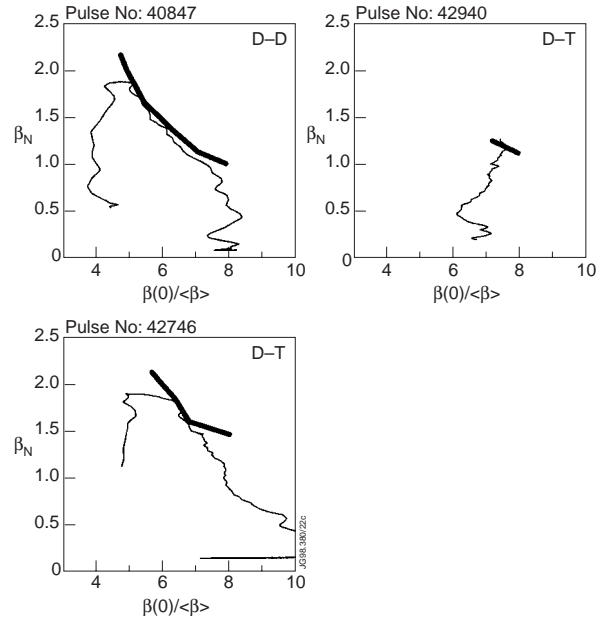


FIG. 20. Time evolution of β_N for typical D-D and D-T plasma pulses compared with the unstable region calculated for the $n = 1$ ideal pressure driven kink mode [47]. Generally, power is controlled to avoid disruption (not successful for pulse No. 42940).

5.4. Simultaneous Internal and Edge Transport Barriers

The highest fusion performance was normally obtained by prolonging the phase during which the plasma edge was in L-mode; the subsequent ELM-free H-mode phase made these discharges transient. A significant number of discharges, however, developed both an ITB and an ELMy H-mode edge [43] as illustrated in Fig. 21, with a substantial fusion yield being produced. In pulse No. 42733, an ITB is formed and the central ion temperature reaches 24 keV, while the edge ion temperature is about 3 keV, typical of an ELMy H-mode plasma. Such double barrier discharges show great potential for steady-state operation.

In pulse No. 42733 the fusion power increases from the start of the main heating phase until it reaches 6.8 MW, at which time the input power is reduced to economise on D-T neutrons. This increase in fusion yield is due to a continuous build-up of central density together with an increase of the tritium concentration. The stored plasma energy reaches 8.8 MJ for a total injected power of 18.4 MW and a corresponding confinement enhancement factor $H_{89} \approx 2.3$

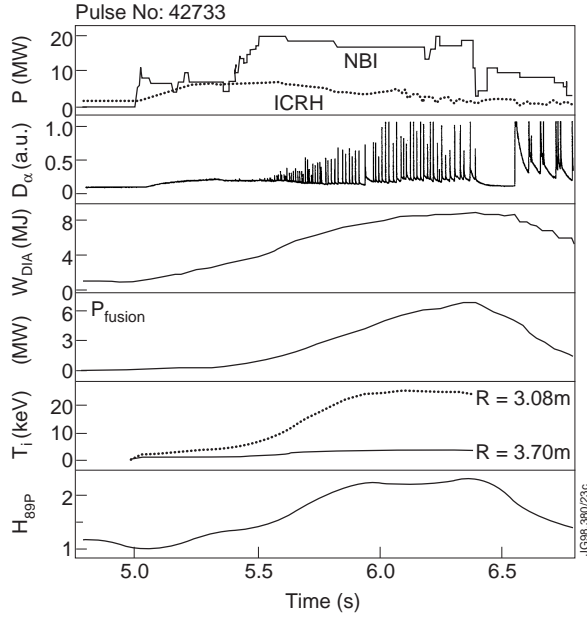


FIG. 21. Time history of pulse No. 42733 which develops an Internal Transport Barrier with an ELM-free H-mode edge. $B_T = 3.4$ T and the I_p is ramped from 2.3 MA at $t = 4.8$ s to 3 MA at $t = 6.3$ s. The power was stepped down to limit the number of 14 MeV neutrons.

5.5. Stability of Alfvén Eigenmodes

In the optimised shear scenario, AEs are found to be always unstable, due to the presence of a large high energy tail generated by the high ICRF heating power typically required to produce the ITB in this regime. The most favourable scenario for the observation of alpha particle effects on AEs is created by suddenly switching off the auxiliary heating [50]. AE activity is observed around 0.5 s into the “after-glow” phase of some of these discharges. Stability calculations performed by the CASTOR-K model show that, after a few hundreds of milliseconds into the after-glow, the drive from slowing down alpha particles can overcome the damping mechanisms for the AEs. However, the presence of a slowing down tail of ICRF generated ions provides an additional drive which can be comparable with the alpha particle drive. A definitive identification of the additional contribution of the alpha particles to the ICRF-drive is very difficult due to uncertainties in the ICRF-drive calculations.

6. SUMMARY, CONCLUSIONS AND OUTLOOK

The main results of the paper are now placed in the wider context of present tokamak research, the future JET programme and the final goal of a fusion reactor.

The ELM-free H-mode has been the established route to high performance, setting world records in fusion performance, validating D-D projections of D-T performance, and demonstrating clear alpha particle heating. The experiments not only led to 16.1 MW of fusion power

relative to the ITER89-P scaling [49]. In this pulse, as in similar D-T and D-D pulses, the positions of the $q = 2$ magnetic surface and the ITB change only slowly with time; this is a consequence of the generation of an edge bootstrap current. At 6.3 s, the power was stepped down and it is interesting to note that the subsequent collapse of the ITB triggers an ELM-free H-mode.

This route, which could not be explored further during DTE1 due to the imposed constraint on the number of D-T neutrons produced, shows significant promise for steady-state high fusion yield D-T plasmas, but would require a technique for better control of the plasma edge and/or current profile.

and transient values of $Q_{\text{tot}}^{\text{P}}$ of 0.95 ± 0.17 , consistent with the high values of $n_{\text{DT}}(0) \tau_{\text{E}}^{\text{dia}} T_i(0) = 8.7 \times 10^{20} \text{ m}^{-3} \text{ s keV}$, but also demonstrated the expected factor of 210 between D-D and D-T fusion power, confirming the quality of the JET kinetic data and the physics contained within TRANSP.

The high values of Q correspond to high values of $P_{\alpha}/P_{\text{loss}} \approx 16\%$, so that the alpha particle heating becomes a measurable contribution to the power balance. Indeed the alpha particle heating produced a rise in electron temperature of order 1 keV per Megawatt of alpha particle heating, clearly separated from isotope effects which were shown to be very small. This behaviour is consistent with the classical alpha particle power deposition profiles.

The mixture control experiments enabled an optimum D-T plasma mix to be achieved (even with a non-optimal NB mix) and played a crucial role in the success of the ELM-free H-mode programme in D-T. The methodology developed is of general application and will be of value to future D-T experiments on JET and elsewhere.

High performance ELM-free H-mode plasmas were limited by giant ELMs to $\beta_{\text{N}} \approx 2.2$, thus preventing Q_{in} from exceeding 0.64. This value of β_{N} is lower than the expected Troyon limit ($\beta_{\text{N}} \approx 2.8$) because the pressure profile is flatter than the optimum and the limit is set by a steep pressure gradient in the plasma edge. On the other hand, in regimes with more peaked pressure profiles such as the TFTR supershot regime or the optimised shear regime discussed in Section 5, β_{N} is limited to ≈ 1.9 by MHD instabilities associated with the steep pressure gradients in the plasma core.

The different plasma conditions obtained in the supershot and ELM-free H-mode regimes have allowed complementary fusion studies to be pursued. In the TFTR supershot, higher input powers and peaked pressure profiles led to a higher central fusion power density which has been exploited for the investigation of MHD effects (including sawteeth) on alpha particles. In the JET ELM-free H-mode, better confinement led to a higher fusion power and Q and clearly visible alpha particle heating (despite flatter pressure profiles), with the highest electron temperature showing a clear correlation with the maximum alpha particle heating power and the optimum ($\approx 40:60$) D-T mixture. This demonstration of alpha particle heating, in conditions where there is no isotope effect on energy confinement and TAEs are stable (in agreement with predictions), reveals no unexpected effects which might prevent ignition in a larger device. A study of alpha particle heating in the presence of alpha particle driven TAEs would require a factor of two increase in β_{α} above that obtained so far in JET hot ion H-mode discharges.

The optimised shear regime is less mature than either the ELM-free H-mode or the supershot mode, but has the potential for combining the best features of both these regimes and to further the study of alpha particle physics. Substantial progress was made during the scenario development which led to the production of 8.2 MW of fusion power. First, and most importantly, strong internal transport barriers were shown to exist in D-T. These barriers could be established with similar powers to those required in D-D, in contrast to the edge H-mode barrier whose threshold

is lower in D-T. Second, the poor mixture control and reduced core fuelling by NB injection (tritium concentration only 30%) limited the fusion performance, but was related to short term technical constraints rather than to a fundamental deficiency. Future JET experiments would benefit from tritium injection from both NB injectors and the methodology for optimising the plasma mixture applied successfully to the ELM-free H-mode could then also be adopted. Third, the evolution of the pressure profile peaking was successfully controlled very close to the maximum permitted by pressure gradient driven stability in D-D, but could not be optimised in D-T ($\beta_N \approx 1.9$). It is reasonable to conclude that, given sufficient experimental time and D-T neutron budget, this regime should deliver the fusion performance and Q commensurate with the high values of the fusion triple product ($n_{DT}(0)\tau_E T_i(0) \approx 10^{21} \text{ m}^{-3} \text{ s keV}$) demonstrated.

The high performance regimes considered in this paper would be even more reactor-relevant if they could be maintained in steady-state. To realise the potential suggested by the high values of Q_{tot}^P obtained in the ELM-free H-mode would require exercising control over the steep gradients in the edge transport barrier which have led, so far, inexorably towards instability. Such control would also be required for scenarios in which an internal transport barrier co-existed with an ELM-free H-mode edge, since high performance is then also terminated by a giant ELM. A pressure profile intermediate between that of the ELM-free H-mode and the optimised shear regime with an internal transport barrier and an L-mode edge would be required. Such pressure profiles are to be found in discharges in which an internal transport barrier has been obtained simultaneously with an ELMy H-mode edge, as already observed in D-D on JET, JT60-U and DIII-D, and in D-T on JET [43]. This scenario could offer an alternative for steady-state high fusion performance to the standard ELMy H-mode (the presently established scenario for ITER), but would require high β_p (plasma pressure normalised to the pressure of the poloidal magnetic field) for steady-state operation and high β_N together with high confinement for high performance. Calculations show that such discharges on JET can be MHD stable up to $\beta_N = 2.5$ [47] and further optimisation of the current profile can even lead to stable β_N values in excess of 3 [51]. This would require not only edge control to maintain non-disruptive edge pressure gradients (e.g. using current ramps or impurity radiation at the edge), but also careful current profile control in addition to the pressure profile control already demonstrated to avoid pressure driven disruptions at high β_N . The achievement of such high performance conditions and a double transport barrier would allow the effects of ELMs on alpha particle behaviour to be investigated with the presently available additional heating, whereas ELMy H-mode plasmas without an internal transport barrier would require a significant increase in heating power for such studies.

The D-T results presented in this and the companion [9] paper confirm a mature understanding of H-mode plasmas and indicate significant progress towards the achievement of a similar level of understanding of plasmas with internal transport barriers. The significant progress in understanding made over the years in tokamak fusion physics can now be exploited in JET and future devices to advance the realisation of a tokamak fusion reactor.

REFERENCES

- [1] JET TEAM, Nucl. Fusion **32** (1992) 187.
- [2] JET TEAM (presented by D. STORK), in Plasma Physics and Controlled Nuclear Fusion Research 1994 (Proc. 15th Int. Conf. Seville, Spain, 1994), Vol. 1, IAEA, Vienna (1995) 51.
- [3] AYMAR, R. et al., in Fusion Energy 1996 (Proc. 16th Int. Conf. Montreal, Canada, 1996) Vol. 1, IAEA, Vienna (1997) 3.
- [4] McGUIRE, K., M. and the TFTR TEAM, in Fusion Energy 1996 (Proc. 16th Int. Conf. Montreal, Canada, 1996) Vol. 1, IAEA, Vienna (1997) 19.
- [5] LEVINGTON, F., M. et al., Phys. Rev. Lett. **75** (1995) 4417.
- [6] SCOTT, S. D. et al., in Fusion Energy 1996 (Proc. 16th Int. Conf. Montreal, Canada, 1996) Vol. 1, IAEA, Vienna (1997) 573.
- [7] LÄSSER, R. D. et al., 17th IEEE/NPSS Symposium on Fusion Engineering, San Diego, California, October 1997, Vol. I, p. 292 (1997).
- [8] JET TEAM (presented by G.C. VLASES), in Fusion Energy 1996 (Proc. 16th Int. Conf. Montreal, Canada, 1996) Vol. 1, IAEA, Vienna (1997) 371.
- [9] JACQUINOT, J. et al. and the JET TEAM, "Overview of ITER Physics Deuterium- Tritium Experiments in JET", accepted for publication in Nucl. Fusion (1998).
- [10] ANDREW, P. et al., Nucl. Fusion **33** (1993) 1389.
- [11] PEACOCK, A. et al., 13th Int. Conf. on Plasma Surface Interactions, San Diego, California, May 1998, to be published in J. Nucl. Materials (1998).
- [12] BALET, B. et al., Nucl. Fusion **33** (1993) 1345.
- [13] NAVE, M. F. F. et al., Nucl. Fusion **37** (1997) 809.
- [14] JET TEAM (presented by P. J. LOMAS), in Plasma Physics and Controlled Nuclear Fusion Research 1994 (Proc. 15th Int. Conf. Seville, Spain, 1994), Vol. 1, IAEA, Vienna (1995) 211.
- [15] HUYSMANS, G. T. A. et al., Nucl. Fusion **38** (1998) 179.
- [16] LOMAS, P. J. et al., "Performance of the ELM-free H-mode in DD and DT: The Realisation of Significant Fusion Power", in preparation (1998).
- [17] MARCUS, F. B. et al., Nucl. Fusion **33** (1993) 1325.
- [18] JET TEAM (presented by P. J. LOMAS), in Fusion Energy 1996 (Proc. 16th Int. Conf. Montreal, Canada, 1996) Vol. 1, IAEA, Vienna (1997) 239.
- [19] JONES, T. T. C. et al., to be published in Proc. 25th Eur. Conf. on Controlled Fusion and Plasma Physics, Prague, Czech Rep., June 1998, by European Physical Society, Geneva (1998).
- [20] RIMINI, F. G. et al., "Combined Heating Experiments in ELM-free H-modes in JET", in preparation (1998).
- [21] NAVE, M. F. F. et al., "Discharge Optimisation and Control of MHD-Modes", in preparation (1998).

- [22] GIBSON, A. and the JET TEAM, *Physics of Plasmas* **5** (1998) 1839.
- [23] FASOLI, A. et al., *Plasma Phys. Control. Fusion* **39** (1997) B287.
- [24] SHARAPOV, S.E. et al., “Stability of Alpha Particle Driven Alfvén Eigenmodes in High Performance JET D-T Plasmas”, submitted to *Nucl. Fusion* (1998).
- [25] NAZIKIAN, R. and FU, G.Y., *Phys. Rev. Lett.* **78** (1997) 2976.
- [26] KRAMER, G.J., SAIGUSA, M. et al., *Phys. Rev. Lett.* **80** (1998) 2594.
- [27] HEIDBRINK, W. and SADLER, G. J., *Nucl. Fusion* **34** (1994) 535.
- [28] TAYLOR, G. et al., *Phys. Rev. Lett.* **76** (1996) 2722.
- [29] THOMAS, P.R. et al., *Phys. Rev. Lett.* **80** (1998) 5548.
- [30] NAVE, M. F. F. et al., to be published in *Proc. 25th Eur. Conf. on Controlled Fusion and Plasma Physics, Prague, Czech Rep., June 1998*, by European Physical Society, Geneva (1998).
- [31] START, D. F. H. et al., *Proc. 17th EPS Conf. on Controlled Fusion and Plasma Heating, Amsterdam, June 1990, Part III, Vol. 14B*, p. 1019.
- [32] JACQUINOT, J. et al., *Plasma Phys. Control. Fusion* **30** (1988) 1467.
- [33] HUGON, M. et al., *Nucl. Fusion* **32** (1992) 33.
- [34] KESSEL, C. et al., *Phys. Rev. Lett.* **72** (1994) 1212.
- [35] STRAIT, E. J. et al., *Phys. Rev. Lett.* **75** (1995) 4421.
- [36] USHIGUSA, K., and the JT-60 TEAM, in *Fusion Energy 1996 (Proc. 16th Int. Conf. Montreal, Canada, 1996) Vol. 1, IAEA, Vienna (1997)* 37.
- [37] JET TEAM (presented by C. GORMEZANO), in *Fusion Energy 1996 (Proc. 16th Int. Conf. Montreal, Canada, 1996) Vol. 1, IAEA, Vienna (1997)* 487.
- [38] PARAIL, V. et al., “Predictive Modelling of JET Optimised Shear Discharges”, submitted to *Nucl. Fusion* (1998).
- [39] SIPS, A. C. C. et al., *Plasma Phys. Control. Fusion* **40** (1998) 1171.
- [40] COTTRELL, G. A. et al., in *Controlled Fusion and Plasma Physics (Proc. 24th Eur. Conf. Berchtesgaden, Germany, 1997)*, European Physical Society, Geneva (1997) Part I, Vol. **21A**, 81.
- [41] COTTRELL, G.A. et al., “ICRF Heating of JET Plasmas with Optimised Shear”, submitted to *Nucl. Fusion* (1998).
- [42] JET TEAM (presented by F. X. SÖLDNER), *Plasma Phys. Control. Fusion* **39** (1997) B353.
- [43] SÖLDNER, F.X. et al., “Towards Steady-State High Performance with Optimised Shear”, submitted to *Nucl. Fusion* (1998).
- [44] JET TEAM (presented by M. KEILHACKER), *Plasma Phys. Control. Fusion* **39** (1997) B1.
- [45] JET TEAM (presented by J. JACQUINOT), in *Controlled Fusion and Plasma Physics (Proc. 24th Eur. Conf. Berchtesgaden, Germany, 1997)*, European Physical Society, Geneva (1997), Part IV, Vol. **21A**, 1865.

- [46] GORMEZANO, C. et al., Phys. Rev. Lett. **80** (1998) 5544.
- [47] HUYSMANS, G. T. A., et al., in Controlled Fusion and Plasma Physics (Proc. 24th Eur. Conf. Berchtesgaden, Germany, 1997), European Physical Society, Geneva (1997), Part I, Vol. **21A**, 21.
- [48] HINTON, F.L. and HAZELTINE, R.D., Rev. Modern Physics **48** (1976) 239.
- [49] SCHISSEL, D.P. et al., Nucl. Fusion **31** (1991) 73.
- [50] BUDNEY, R. V. et al., Nucl. Fusion **32** (1992) 429.
- [51] BONDESON, A. et al, Nucl. Fusion **37** (1997) 1419.

Appendix I

THE JET TEAM

JET Joint Undertaking, Abingdon, Oxon, OX14 3EA, U.K.

J.M. Adams¹, P. Ageladarakis, B. Alper, H. Altmann, V. Amasov³, S. Arshad, P. Andrew, Y. Andrew¹², D. Bailey, N. Bainbridge, B. Balet, Y. Baranov⁸, P. Barker, R. Barnsley², M. Baronian, D.V. Bartlett, A.C. Bell, L. Bertalot¹⁰, E. Bertolini, V. Bhatnagar, A.J. Bickley, H. Bindslev, K. Blackler, D. Bond, T. Bonicelli, D. Borba¹⁹, M. Brandon, P. Breger, H. Brelen, P. Brennan, W.J. Brewerton, M.L. Browne, T. Budd, R. Budny¹⁴, A. Burt, T. Businaro, M. Buzio, C. Caldwell-Nichols, D. Campling, P. Card, C.D. Challis, A.V. Chankin, D. Chiron, J. Christiansen, P. Chuilon, D. Ciric, R. Claesen, H.E. Clarke, S. Clement, J.P. Coad, I. Coffey⁷, S. Conroy¹⁶, G. Conway¹⁷, S. Cooper, J.G. Cordey, G. Corrigan, G. Cottrell, M. Cox⁷, S.J. Cox, R. Cusack, N. Davies, S.J. Davies, J.J. Davis, M. de Benedetti, H. de Esch, J. de Haas, E. Deksnis, N. Deliyankis, A. Dines, S.L. Dmitrenko, J. Dobbing, N. Dolgetta, S.E. Dorling, P.G. Doyle, H. Duquenoy, A.M. Edwards⁷, A.W. Edwards, J. Egedal, J. Ehrenberg, A. Ekedahl¹¹, T. Elevant¹¹, J. Ellis, M. Endler¹³, S.K. Erents⁷, G. Ericsson¹⁶, B. Esposito¹⁰, L.G. Eriksson, H. Falter, J.W. Farthing, M. Fichtmüller, G. Fishpool, K. Fullard, M. Gadeberg, L. Galbiati, A. Gibson, R.D. Gill, D. Godden, A. Gondhalekar, D. Goodall⁷, C. Gormezano, C. Gowers, M. Groth¹⁸, K. Guenther, H. Guo, A. Haigh, B. Haist⁴, C.J. Hancock, P.J. Harbour, N.C. Hawkes⁷, N.P. Hawkes¹, J.L. Hemmerich, T. Hender⁷, J. Hoekzema, L. Horton, A. Howman, M. Huart, T.P. Hughes, F. Hurd, G. Huysmans, C. Ingesson¹⁵, B. Ingram, M. Irving, J. Jacquinet, H. Jaeckel, J.F. Jaeger, O.N. Jarvis, M. Johnson, E.M. Jones, T.T.C. Jones, J-F. Junger, F. Junique, C. Jupen, J. Kallne¹⁶, A. Kaye, B.E. Keen, M. Keilhacker, W. Kerner, N.G. Kidd, S. Knipe, R. Konig, A. Korotkov, A. Krasilnikov³, J.G. Krom, P. Kupschus, R. Lässer, J.R. Last, L. Lauro-Taroni, K. Lawson⁷, M. Lennholm, J. Lingertat, X. Litaudon²¹, T. Loarer, P.J. Lomas, M. Loughlin, C. Lowry, A.C. Maas¹⁵, B. Macklin, C.F. Maggi, M. Mantsinen⁵, V. Marchese, F. Marcus, J. Mart, D. Martin, G. Matthews, H. McBryan, G. McCracken, P.A. McCullen, A. Meigs, R. Middleton, P. Miele, F. Milani, J. Mills, R. Mohanti, R. Monk, P. Morgan, G. Murphy, F. Nave¹⁹, G. Newbert, P. Nielsen, P. Noll, W. Obert, D. O'Brien, M. O'Mullane, E. Oord, R. Ostrom, S. Papastergiou, V.V. Parail, R. Parkinson, W. Parsons, B. Patel, A. Paynter, A. Perevezentsev, A. Peacock, R.J.H. Pearce, M.A. Pick, J. Plancoulaine, O. Pogutse, R. Prentice, S. Puppini, G. Radford⁹, R. Reichle, V. Riccardo, F. Rimini, F. Rochard²¹, A. Rolfe, A.L. Roquemore¹⁴, R.T. Ross, A. Rossi, G. Sadler, G. Saibene, A. Santagiustina, R. Sartori, R. Saunders, P. Schild, M. Schmid, V. Schmidt, B. Schokker¹⁵, B. Schunke, S.M. Scott, S. Sharapov, A. Sibley, M. Simon, R. Simonini, A.C.C. Sips, P. Smeulders, P. Smith, R. Smith, F. Söldner, J. Spence, E. Springmann, R. Stagg, M. Stamp, P. Stangeby²⁰, D.F. Start, D. Stork, P.E. Stott, J.D. Strachan¹⁴, P. Stubberfield, D. Summers, L. Svensson, P. Svensson, A. Tabasso¹², M. Tabellini, J. Tait, A. Tanga, A. Taroni, C. Terella, P.R. Thomas, K. Thomsen, E. Traneus¹⁶, B. Tubbing, P. Twyman, A. Vadgama, P. van Belle, G.C. Vlases, M. von Hellermann, T. Wade, R. Walton, D. Ward, M.L. Watkins, N. Watkins¹, M.J. Watson, M. Wheatley, D. Wilson, T. Winkel, D. Young, I.D. Young, Q. Yu⁶, K-D. Zastrow, W. Zwingmann.

PERMANENT ADDRESSES

1. UKAEA, Harwell, Didcot, Oxon, UK.
2. University of Leicester, Leicester, UK.
3. TRINITY, Troitsk, Moscow, Russia.
4. KFA, Jülich, Germany.
5. Helsinki University of Technology, Espoo, Finland.
6. Institute of Plasma Physics, Hefei, P R of China.
7. UKAEA Culham Laboratory, Abingdon, Oxon, UK.
8. A.F. Ioffe Institute, St. Petersburg, Russia.
9. Institute of Theoretical Physics, University of Oxford, UK.
10. ENEA, CRE Frascati, Roma, Italy.
11. Royal Institute of Technology, Stockholm, Sweden.
12. Imperial College, University of London, UK.
13. Max Planck Institut für Plasmaphysik, Garching, Germany.
14. Princeton Plasma Physics Laboratory, Princeton, USA.
15. FOM Instituut voor Plasmafysica, Nieuwegein, The Netherlands.
16. Dept. of Neutron Research, Uppsala University, Sweden.
17. University of Saskatchewan, Saskatoon, Canada.
18. University of Manchester Institute of Science and Technology, Manchester, UK.
19. IST, Centro de Fuso Nuclear, Lisbon, Portugal.
20. Institute for Aerospace Studies, University of Toronto, Canada.
21. CEA, Cadarache, France.